ouabain-induced ACh release was suppressed by TTX and ω-conotoxin MVIIC, indicating that ouabain-induced depolarization and subsequently ACh release via P/Q type $Ca^{2+}$ channel opening. TTX sensitive or resistant response may be interpreted as two different types of neurotransmitter release mechanisms. Alternatively, ouabain may have induced increases in intraneuronal $Na^+$ accumulation and elevation of extraneuronal $K^+$ levels by inhibition of $Na^+$,$K^+$-ATPase (D'Ambrosio *et al.* 2002). Elevations of both intracellular $Na^+$ and extracellular $K^+$ exerted regional depolarization following exocytosis via different mechanisms. In the previous study, we demonstrated that high $K^+$-induced NA release was insensitive to TTX but sensitive to ω-conotoxin GVIA. Furthermore, high $K^+$ caused a marked increase in dialysate NA but little increase in dialysate Ach (Yamazaki *et al.* 1998, Kawada *et al.* 2001). Thus high $K^+$-induced neurotransmitter release might greatly contribute to the increase in dialysate NA evoked by ouabain but might contribute little to the increase in dialysate ACh.

In conclusion, ouabain alone causes a brisk efflux of NA and ACh from cardiac sympathetic and parasympathetic nerve endings respectively. The ouabain-induced ACh release contributes to the mechanism of ACh exocytosis, which is triggered by centrally mediated or regional depolarization. The regional exocytosis is caused by opening of P/Q type $Ca^{2+}$ channels and/or intracellular $Ca^{2+}$ mobilization from the stored ACh vesicle. The ouabain-induced NA release contributes to the mechanisms of regional exocytosis and/or carrier-mediated outward transport of NA, from stored NA vesicle and/or axoplasma respectively. The regional exocytosis is caused by opening of N type $Ca^{2+}$ channels and intracellular $Ca^{2+}$ mobilization.

## Conflict of interest

None.

This work was supported by Grants-in-Aid for scientific research (17591659) from the Ministry of Education, Culture, Sports, Science and Technology.

## References

Akiyama, T., Yamazaki, T. & Ninomiya, I. 1991. *In vivo* monitoring of myocardial interstitial norepinephrine by dialysis technique. *Am J Physiol* 261, H1643–H1647.

Akiyama, T., Yamazaki, T. & Ninomiya, I. 1994. *In vivo* detection of endogenous acetylcholine release in cat ventricles. *Am J Physiol* 266, H854–H860.

Calabresi, P., Marfia, G.A., Centonze, D., Pisani, A. & Bernardi, G. 1999. Sodium influx plays a major role in the membrane depolarization induced by oxygen and glucose deprivation in rat striatal spiny neurons. *Stroke* 30, 171–190.

Casali, T.A., Gomez, R.S., Moraes-Santos, T. & Gomez, M.V. 1995. Differential effects of calcium channel antagonists on tityustoxin and ouabain-induced release of [3H] acetylcholine from brain cortical slices. *Neuropharmacology* 34, 599–603.

D'Ambrosio, R., Gordon, D.S. & Winn, H.R. 2002. Differential role of KIR channel and Na(+)/K(+)-pump in the regulation of extracellular K(+) in rat hippocampus. *J Neurophysiol* 87, 87–102.

Dierkes, P.W., Wusten, H.J., Klees, G., Muller, A. & Hochstrate, P. 2006. Ionic mechanism of ouabian-induced swelling of leech Retzius neurons. *Pflugers Arch* 452, 25–35.

Edward, C., Dolezal, D., Tucek, S., Zemkova, H. & Vyskocil, F. 1985. Is an acetylcholine transport system responsible for nonquantal release of acetycholine at the rodent myoneural junction? *Proc Natl Acad Sci USA* 82, 3514–3518.

Gillis, R.A. & Quest, J.A. 1979. The role of the nervous system in the cardiovascular effects of digitalis. *Pharmacol Rev* 31, 19–97.

Gomez, R.S., Gomez, M.V. & Prado, M.A.M. 1996. Inhibition of $Na^+$, $K^+$-ATPase by ouabain opens calcium channels coupled to acetylcholine release in guinea pig myenteric plexus. *J Neurochem* 66, 1440–1447.

Haass, M., Serf, C., Gerber, S.H. *et al.* 1997. W. Dual effect of digitalis glycoside on norepinephrine release from human atrial tissue and bovine adrenal chromaffin cells: differential dependence on $[Na+]_i$ and $[Ca2+]_i$. *J Mol Cell Cardiol* 29, 1615–1627.

Katsuragi, T., Ogawa, S. & Furukawa, T. 1994. Contribution of intra-and extracellular $Ca^{2+}$ to noradrenaline exocytosis induced by ouabain and monesin from guinea-pig vas deferens. *Br J Pharmacol* 113, 795–800.

Kawada, T., Yamazaki, T., Akiyama, T. *et al.* 2006. Effects of Ca2+ channel anatagonists on nerve stimulation-induced and ischemia-induced myocardial interstitial acetylcholine release in cats. *Am J Physiol* 291, H2181–2191.

Kawada, T., Yamazaki, T., Akiyama, T. *et al.* 2001. *In vivo* assessment of acetylcholine-releasing function at cardiac vagal nerve terminals. *Am J Physiol* 281, H139–H145.

Kranzhöfer, R., Haass, M., Kurz, T., Richardt, G. & Schömig, A. 1991. Effect of digitalis glycosides on norepinephrine release in the heart: dual mechanism of action. *Circ Res* 68, 1628–1637.

McIvor, M.E. & Cummings, C.C. 1987. Sodium fluoride produces a K+ efflux by increasing intracellular Ca2+ through Na+-Ca2+ exchange. *Toxicol Lett* 38, 169–176.

Nikolsky, E.E., Voronin, V.A. & Vyskocil, F. 1991. Kinetic differences in the effect of calcium on quantal and non-quantal acetylcholine release at the murine diaphragm. *Neurosci Lett* 123, 192–194.

Nishio, M., Ruch, S.W., Kelly, J.E., Aistrup, G.L., Sheehan, K. & Wasserstrom, J.A. 2004. Ouabain increases sarcoplasmic reticulum calcium release in cardiac myocytes. *J Pharmacol Exp Ther* 308, 1181–1190.

Satoh, E. & Nakazato, Y. 1992. On the mechanisim of ouabain-induced release of acetylcholine from synaptsomes. *J Neurochem* 58, 1038–1044.

Sharma, V.K., Pottick, L.A. & Banerjee, S.P. 1980. Ouabain stimulation of noradrenaline transport in guinea pig heart. *Nature* 286, 817–819.

 doi: 10.1111/j.1748-1716.2007.01749.x 

Smith, D.O. 1992. Routes of actylcholine leakage from cytosolic and vesicular compartments of rat motor nerve terminals. *Neurosci Lett* 135, 5–9.

Sweadner, K. 1985. Ouabain-evoked norepinephrine release from intact rat sympathetic neurons: evidence for carrier-mediated release. *J Neurosci* 5, 2397–2406.

Verbny, Y., Zhang, C.L. & Chiu, S.Y. 2002. Coupling of calcium homeostasis to axonal sodium in axons of mouse optic nerve. *J Neurophysiol* 88, 802–816.

Vizi, E.S. 1998. Differential temperature dependence of carrier-mediated (cytoplasmic) and stimulus-evoked (exocytotic) release of transmitter: a simple method to separate two types of relase. *Neurochem Int* 33, 359–366.

Vyskocil, F. & Illes, P. 1977. Non-quantal release of transmitter at mouse neuromuscular junction and its dependency on the activity of $Na^+$-$K^+$ ATPase. *Pflugers Arch* 370, 295–297.

Wasserstrom, J.A. & Aistrup, G.L. 2005. Digitalis: new actions for an old drug. *Am J Physiol Heart Circ Physiol* 289, H1781–H1793.

Wiedenkeller, D.E. & Sharp, G.W. 1984. Unexpected potentiation of insulin release by the calcium store blocker TMB-8. *Endocrinolgy* 114, 116–119.

Yamazaki, T., Akiyama, T., Kitagawa, H., Takauchi, Y., Kawada, T. & Sunagawa, K. 1997. A new, concise dialysis approach to assessment of cardiac sympathetic nerve terminal abnormalities. *Am J Physiol* 272, H1182–H1187.

Yamazaki, T., Akiyama, T., Kawada, T. *et al.* 1998. Norepinephrine efflux evoked by potassium chloride in cat sympathetic nerves: dual mechanism of action. *Brain Res* 794, 146–150.

Yamazaki, T., Akiyama, T. & Mori, H. 2001. Effects of nociceptin on cardiac norepinephrine and acetylcholine release evoked by ouabain. *Brain Res* 904, 153–156.

Zemkova, H., Vyskocil, F. & Edwards, C. 1990. The effect of nerve terminal activity on non-quantal release of acetylcholine at the mouse neuromuscular junction. *J Physiol* 423, 631–640.

# Single Injection of a Sustained-release Prostacyclin Analog Improves Pulmonary Hypertension in Rats

Hiroaki Obata[1,2], Yoshiki Sakai[3], Shunsuke Ohnishi[1], Satoshi Takeshita[4], Hidezo Mori[5], Makoto Kodama[2], Kenji Kangawa[6], Yoshifusa Aizawa[2], and Noritoshi Nagaya[1,4]

[1]Department of Regenerative Medicine and Tissue Engineering, National Cardiovascular Center Research Institute, Osaka, Japan; [2]Division of Cardiology, Niigata University Graduate School of Medical and Dental Science, Niigata, Japan; [3]Ono Pharmaceutical Co. Ltd., Research Headquarters, Osaka, Japan; [4]Department of Internal Medicine, National Cardiovascular Center, Osaka, Japan; [5]Department of Cardiac Physiology, National Cardiovascular Center Research Institute, Osaka, Japan; and [6]Department of Biochemistry, National Cardiovascular Center Research Institute, Osaka, Japan

*Rationale*: Although prostacyclin is recognized as a therapeutic breakthrough for pulmonary hypertension, it needs continuous infusion because of its short action. Therefore, we developed a new drug delivery system for prostacyclin. We prepared ONO-1301MS, a novel sustained-release prostacyclin analog polymerized with poly(D, L-lactic-co-glycolic acid) (PLGA) microspheres.

*Objectives*: We examined whether ONO-1301MS attenuates monocrotaline (MCT)-induced pulmonary hypertension in rats, and attempted to elucidate the underlying mechanisms responsible for the beneficial effects of ONO-1301MS.

*Methods*: After MCT injection, rats were randomized to receive a single subcutaneous injection of 100 mg/kg ONO-1301MS or vehicle.

*Measurements and Main Results*: We prepared ONO-1301MS, which was polymerized with PLGA to release ONO-1301 for 3 weeks. A single administration of ONO-1301MS achieved sustained elevation of its circulating level and plasma cyclic adenosine 3′,5′-monophosphate level for 3 weeks, and attenuated an increase in a metabolite of thromboxane $A_2$ level. Rats had developed pulmonary hypertension 3 weeks after MCT injection; however, treatment with ONO-1301MS significantly attenuated the increases in right ventricular systolic pressure and right ventricular weight to body weight ratio. ONO-1301MS significantly inhibited hypertrophy of pulmonary arteries. Phosphorylation of extracellular signal-regulated protein kinase (ERK) in the lung was significantly increased in the control group, whereas this increase was markedly attenuated by treatment.

*Conclusions*: We developed a new drug delivery system for prostacyclin using PLGA and ONO-1301. A single injection of ONO-1301MS resulted in sustained activity for 3 weeks, and attenuated pulmonary hypertension, partly through its antiproliferative effect on vascular smooth muscle cells via inhibition of ERK phosphorylation.

Keywords: pulmonary hypertension; prostacyclin analog; sustained-release preparation; extracellular signal regulated kinase; poly(lactic-co-glycolic acid)

### AT A GLANCE COMMENTARY

**Scientific Knowledge on the Subject**

Although prostacyclin is recognized as a therapeutic breakthrough for pulmonary hypertension, it needs continuous infusion because of its short action. For patients with pulmonary hypertension, development of a sustained-release prostacyclin would be beneficial in terms of stable hemodynamics and quality of life.

**What This Study Adds to the Field**

A single injection of ONO-1301MS resulted in sustained activity for 3 weeks, and attenuated pulmonary hypertension in rats.

Pulmonary arterial hypertension is a rare but life-threatening disease characterized by progressive pulmonary hypertension that leads to right ventricular (RV) failure and death (1). Prostacyclin, a metabolite of arachidonic acid, has vasoprotective effects, including vasodilation, antiplatelet aggregation, and inhibition of smooth muscle cell (SMC) proliferation (2–4). Thus, continuous intravenous infusion of prostacyclin (epoprostenol) has become recognized as a therapeutic breakthrough for pulmonary arterial hypertension (5–7). The dramatic success of long-term intravenous prostacyclin has led to the development of prostacyclin analogs (8–11). Nevertheless, treatment with prostacyclin or its analogs has some problems in the clinical setting. Epoprostenol therapy requires a continuous intravenous infusion device, and is therefore more invasive and uncomfortable than taking prostacyclin analogs. On the other hand, prostacyclin analogs, such as subcutaneously infused treprostinil, inhaled iloprost, and oral beraprost, need continuous infusion or frequent administration because of their short duration of action (5–11). In fact, epoprostenol has a very short half-life (<6 min) (12), treprostinil has been reported to have a half-life of 4.6 hours after cessation of continuous subcutaneous infusion (13), iloprost has a serum half-life of 20 to 25 minutes, and the elimination half-life of beraprost is 35 to 40 minutes after oral administration (12).

Recently, we developed a new type of prostacyclin agonist, ONO-1301 (Figure 1), which has long-lasting prostacyclin activity and an inhibitory effect on thromboxane synthase (14). ONO-1301 does not contain prostanoid structures, such as a five-membered ring or allylic alcohol, which are digested by 15-hydroxyprostaglandin dehydrogenase (Figure 1). These structures are considered to be crucial for the stable activity of ONO-1301. This agent is metabolized by cytochrome P450, and the half-life was about 5.6 hours in our previous study (14). In

(*Received in original form March 1, 2007; accepted in final form October 26, 2007*)

Supported by research grants from Ono Pharmaceutical Co., Ltd. (no. 526); Human Genome Tissue Engineering 009 from the Ministry of Health, Labor, and Welfare; the Program for Promotion of Fundamental Studies in Health Science of the National Institute of Biomedical Innovation (NIBIO); and a Grant-in-Aid for Exploratory Research from the Ministry of Education, Culture, Sports, Science, and Technology.

Correspondence and requests for reprints should be addressed to Noritoshi Nagaya, M.D., Department of Regenerative Medicine and Tissue Engineering, National Cardiovascular Center Research Institute, 5-7-1 Fujishirodai, Suita, Osaka 565-8565, Japan. E-mail: nnagaya@ri.ncvc.go.jp

This article contains an online supplement, which is accessible from this issue's table of contents at www.atsjournals.org

Am J Respir Crit Care Med Vol 177. pp 195–201, 2008
Originally Published in Press as DOI: 10.1164/rccm.200703-349OC on November 1, 2007
Internet address: www.atsjournals.org

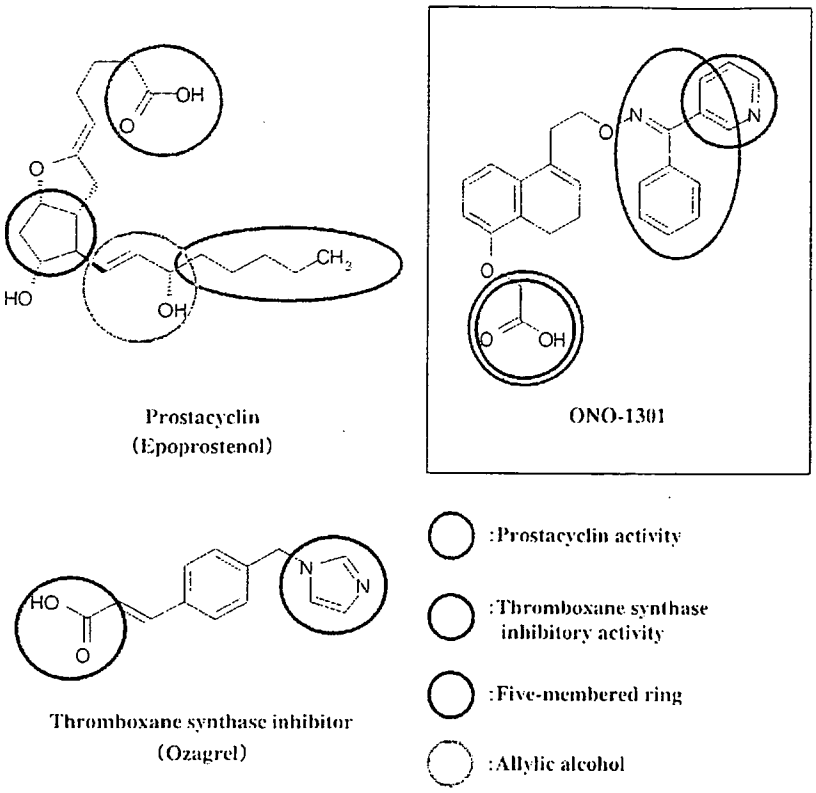


*Figure 1.* Chemical structures of ONO-1301, epoprostenol (prostacyclin analog), and ozagrel (thromboxane synthase inhibitor). Epoprostenol shares common characteristics with prostanoid structures, including a five-membered ring and an allylic alcohol (*blue* and *yellow circles*, respectively). In contrast, ONO-1301 has a carboxylic acid and a lipid-soluble functional group that activates the prostacyclin receptor (*green circles*), but does not have prostanoid structures, which allow long-lasting prostacyclin activity. Unlike epoprostenol, ONO-1301 has thromboxane synthase inhibitory activity because of a 3-pyridine radical and carboxylic acid within its molecule (*red circles*), similar to ozagrel.

addition, ONO-1301 has a 3-pyridine radical, which is known to inhibit thromboxane synthase through interaction with carboxylic acid via a hydrogen bond (Figure 1). Repeated administration of ONO-1301 attenuated monocrotaline (MCT)-induced pulmonary hypertension and improved survival in rats. Although the half-life of plasma ONO-1301 concentration is longer than that of any other prostacyclin analogs, ONO-1301 still needs to be administered twice a day subcutaneously to achieve a significant improvement in pulmonary hypertension. For patients with pulmonary hypertension, development of a long-acting, sustained-release prostacyclin analog would be beneficial in terms of stable hemodynamics and quality of life. To overcome these problems, we developed a new drug delivery system for prostacyclin. We prepared a novel sustained-release prostacyclin analog polymerized with poly(D,L-lactic-co-glycolic acid) (PLGA) microspheres (ONO-1301MS). PLGA microspheres, which are biodegradable and biocompatible compounds, have been used as a controlled delivery system for proteins and drugs (15–20). The release of drug from PLGA microspheres occurs through degradation of the polymeric matrix. Here, we showed that a single subcutaneous administration of ONO-1301MS achieved sustained elevation of its circulating level for 3 weeks.

Thus, the purposes of this study were as follows: (*1*) to investigate whether a single subcutaneous administration of ONO-1301MS attenuates MCT-induced pulmonary hypertension in rats and (*2*) to elucidate the underlying mechanisms responsible for the beneficial effects of this compound.

## METHODS

### Preparation of ONO-1301MS

ONO-1301MS is polymerized ONO-1301 with PLGA microspheres. ONO-1301 and PLGA (polylactic acid to glycolic acid ratio of 50:50) were dissolved in dichloromethane. The dissolved polymer was added to polyvinyl alcohol aqueous solution to form an oil-in-water emulsion. Then, dichloromethane was evaporated by stirring. After centrifugation and washing, ONO-1301MS was isolated by lyophilization.

### Morphologic Studies by Scanning Electron Microscopy

To evaluate the shape and surface morphology of ONO-1301MS, we used a scanning electron microscope (model S-2460N; Hitachi, Tokyo, Japan). After lyophilization, the microspheres were mounted on an aluminum stub and coated with a thin layer (200 Å) of gold by an ion sputter (model E-1010; Hitachi). The surface morphology of the microsphere samples was then visualized under a scanning electron microscope.

### Particle Diameter

ONO-1301MS was suspended in distilled water and dispersed by sonication. The particle diameter was measured by a laser diffraction particle size analyzer (model SALD-2100; Shimadzu, Kyoto, Japan).

### Encapsulation Efficiency

Acetonitrile containing n-propyl 4-hydroxybenzoate served as an internal control to obtain the encapsulation efficiency, and this solution was homogenized by a sonicator. The concentration of ONO-1301 in this solution was analyzed by high-performance liquid chromatography (HPLC). The encapsulation efficiency was calculated as follows:

$$\text{Encapsulation efficiency}(\%) = (\text{measured value}/\text{theoretical value}) \times 100.$$

### *In Vitro* Release of ONO-1301 from PLGA Microspheres

ONO-1301MS was suspended in phosphate-buffered saline (0.067 mol/L salt concentration, pH 6.8) containing 0.2% Tween-80 to adjust the concentration of ONO-1301 to 100 μg/ml. This solution was aliquoted into 1 ml and incubated at 37°C. At various time intervals, one of the aliquots was centrifuged for 5 minutes at 12,000 rpm. The supernatant was discarded, the pellet was dissolved in acetonitrile, and the remaining amount of ONO-1301 was analyzed by HPLC.

### Animal Models

We used 5-week-old male Wistar rats weighing 95 to 110 g. The rats were randomly given a subcutaneous injection of either 60 mg/kg MCT or 0.9% saline, and assigned to receive a subcutaneous injection of 100 mg/kg ONO-1301MS or 0.9% saline. This protocol resulted in the creation of three groups: normal rats given 0.9% saline (sham group, n = 10), MCT rats given 0.9% saline (control group, n = 11), and MCT rats treated with ONO-1301 MS (treated group, n = 11). We chose the maximum dose that did not induce significant hypotension (*see* Figure E1 in the online supplement).

### *In Vivo* Experimental Protocol

After anesthetization by an intraperitoneal injection of 30 mg/kg pentobarbital, rats were given a subcutaneous injection of either 60 mg/kg MCT or 0.9% saline. Subsequently, rats received a single subcutaneous injection of 100 mg/kg ONO-1301MS or 0.9% saline. ONO-1301MS was suspended with 0.9% saline containing 0.2% Tween-80. Hemodynamic measurements and histologic analyses were performed on Day 21. For hemodynamic measurements, rats were anesthetized by intraperitoneal injection of 20 mg/kg pentobarbital, and the following indexes were recorded after an equilibration period. A polyethylene catheter (model PE-50; BD Biosciences, San Jose, CA) was inserted into the right carotid artery to measure heart rate and mean arterial pressure. The catheter was inserted through the right jugular vein into the right ventricle for the measurement of RV pressure. The values of heart rate, mean arterial pressure, and systolic RV pressure were calculated from a series of 20 consecutive heart beats in each rat. Finally, cardiac arrest was induced by injection of 2 mmol/L potassium chloride through the catheter. The ventricles and lungs were excised, dissected free, and weighed. The RV weight to body weight ratio (RV/BW), left ventricular plus septal weight to body weight ratio (LV + S/BW), and RV weight to left ventricular plus septal weight ratio (RV/LV + S) were calculated as indexes of ventricular hypertrophy, as reported previously (21). All protocols were performed in accordance with the guidelines of the Animal Care Ethics Committee of the National Cardiovascular Center Research Institute (Osaka, Japan).

### Morphometric Analysis of Pulmonary Arteries

Paraffin sections of 4-μm thickness were obtained from the lower region of the right lung and stained with hematoxylin and eosin. Analysis of the medial wall thickness of the pulmonary arteries was performed as described previously (22). In brief, the external diameter and the medial wall thickness were measured in 20 muscular arteries (25–100-μm external diameter) per lung section. For each artery, the medial wall thickness was expressed as follows:

$$\%\,\text{wall thickness} = ([\text{medial thickness} \times 2]/\text{external diameter}) \times 100$$

A lung section was obtained from individual rats for comparison among the three groups (n = 5 in each group).

### Assay of Plasma Levels of ONO-1301 and Cyclic AMP

To investigate whether a single subcutaneous administration of ONO-1301MS produces long-lasting prostacyclin activity in rats, we measured plasma levels of ONO-1301 and cyclic AMP (cAMP) after ONO-1301MS injection. Fourteen rats were assigned to receive a single subcutaneous injection of 100 mg/kg ONO-1301MS or 0.9% saline (n = 7 in each group), and blood was drawn from the tail vein on Days 0, 7, 14, and 21. Blood was immediately transferred to a chilled glass tube containing 1 mg/ml disodium ethylenediaminetetraacetic acid and 500 U/ml aprotinin, and centrifuged immediately. Plasma ONO-1301 level was measured by liquid chromatography tandem mass spectrometry assay. Plasma cAMP level was measured with a radioimmunoassay kit (cAMP assay kit; Yamasa Co., Chiba, Japan), as reported previously (23).

### Assay of Urinary Level of 11-Dehydro Thromboxane $B_2$

To investigate the effect of ONO-1301MS on thromboxane synthesis in rats, we measured urinary level of 11-dehydro thromboxane $B_2$ (11-$DTXB_2$), a metabolite of thromboxane $A_2$ ($TXA_2$), after single subcutaneous injection of ONO-1301MS (100 mg/kg) or vehicle (n = 8 in each group). Urine samples were collected for 24 hours on Day 14 by using metabolic cages, and urinary concentration of 11-$DTXB_2$ was measured with an enzyme immunoassay kit (11-$DTXB_2$ assay kit; Cayman Chemical Co., Ann Arbor, MI). The urinary level of 11-$DTXB_2$ was expressed as the ratio of urinary 11-$DTXB_2$ concentration to that of creatinine, as reported previously (24).

### Western Blot Analysis

To investigate the effect of ONO-1301MS on proliferative signaling pathways in homogenized lung tissue, the protein expression of extracellular signal-regulated protein kinase (ERK) 1/2 and phospho-ERK1/2 was determined by Western blotting. Western blotting was performed using rabbit monoclonal antibodies raised against ERK1/2 and phospho-ERK1/2 (Cell Signaling Technology, Danvers, MA). Peripheral samples of lung tissue were obtained on Day 21 from individual rats for comparison among the three groups (n = 6 in each group). Positive protein bands were visualized by means of chemiluminescence (enhanced chemiluminescence kit; Amersham Biosciences, Little Chalfont, UK). Western blot analysis using a mouse polyclonal antibody raised against β-actin (Sigma Chemical Corp., St. Louis, MO) was used as a protein loading control. The resultant bands were quantified using Image J 1.36 imaging software (National Institutes of Health; http://rsb.info.nih.gov/ij/).

### Statistical Analysis

All data were expressed as mean ± SEM. Comparisons of parameters among the three groups were made by one-way analysis of variance (ANOVA), followed by Newman-Keuls test. Comparisons of the time course of parameters between the two groups were made by two-way ANOVA for repeated measures, followed by Newman-Keuls test. A value of $P < 0.05$ was considered statistically significant.

## RESULTS

### Characterization of ONO-1301MS

We prepared three kinds of ONO-1301MS (samples 1, 2, and 3). The external surface morphology of ONO-1301MS (sample 2 as a representative sample) exhibited a spherical shape with a smooth and uniform surface (Figure 2A). The particle size in samples 1, 2, and 3 was 21.2, 42.0, and 71.1 μm, respectively (Figure 2B; sample 2 as a representative sample). Encapsulation efficiency in each sample was 5.1, 21.8, and 17.4%, respectively. *In vitro*, each sample had different time periods of ONO-1301 release at 2, 3, and 4 weeks, respectively (Figure 2C). These data suggest that we were able to vary the release period of ONO-1301.

### Long-lasting Activity of ONO-1301MS

To investigate the pharmacokinetics *in vivo*, we measured plasma ONO-1301 level after a single subcutaneous administration of ONO-1301MS, which was designed to release ONO-1301 for 3 weeks (sample 2). ONO-1301 was detected in plasma for 3 weeks, whereas plasma ONO-1301 level at baseline in the ONO-1301MS group and at all times in the vehicle group was below the detection limit (Figure 3A). In addition, plasma cAMP level after a single subcutaneous administration of ONO-1301MS was significantly higher than that in the control group (Figure 3B). Interestingly, the increase in plasma cAMP level lasted for over 2 weeks in parallel with the change in plasma ONO-1301MS level (Figure 3). These results suggest that subcutaneous administration of ONO-1301MS achieves long-lasting activity in rats.

### Inhibitory Effect of ONO-1301MS on Thromboxane Synthase

Urinary level of 11-$DTXB_2$ was markedly elevated 14 days after MCT injection (Figure 4). However, treatment with ONO-1301MS significantly decreased urinary level of 11-$DTXB_2$ in MCT rats. These results suggest that ONO-1301MS has a sustained inhibitory effect on thromboxane synthase activity.

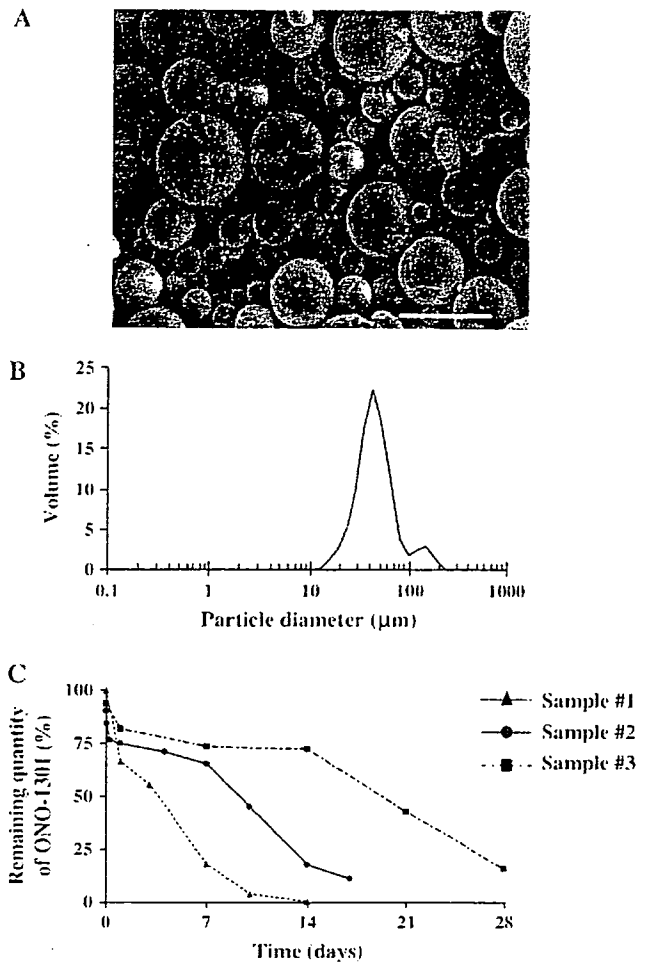


*Figure 2.* Physicochemical characteristics and *in vitro* release of ONO-1301. (*A*) Morphology of ONO-1301MS (sample 2) studied by scanning electron microscopy. *Scale bar* = 50 μm. (*B*) Particle diameter of ONO-1301MS (sample 2) obtained by a laser diffraction particle size analyzer. (*C*) Release profiles of ONO-1301MS in each sample.

### Effects of ONO-1301MS on Pulmonary Hemodynamics and Vascular Remodeling

Three weeks after MCT injection, RV systolic pressure was markedly increased (Figure 5). However, the increase in RV systolic pressure was significantly attenuated in the treated group. Similarly, the increases in RV/BW and RV/LV + S in MCT rats were significantly attenuated by treatment with ONO-1301MS (Figure 5). There were no significant differences in heart rate or mean arterial pressure among the three groups (Table 1). Histologic examination demonstrated that hypertrophy of the pulmonary vascular wall was attenuated in the treated group compared with that in the control group (Figure 6).

No adverse reactions, such as flushing, diarrhea, or hypotension, were observed in the treated group, and there were no significant differences in blood biochemical markers of liver and renal function among the three groups (mean value ± SEM in sham, control, and treated group were, respectively: 139 ± 14, 145 ± 20, and 102 ± 12 IU/L in aspartate aminotransferase; 53 ± 3, 54 ± 5, and 45 ± 3 IU/L in alanine aminotransferase; 0.1 ± 0, 0.1 ± 0, and 0.1 ± 0 mg/dl in total bilirubin; 16.2 ± 1.1, 16.2 ± 0.4, and 15.4 ± 1.2 mg/dl in urea nitrogen; 0.22 ± 0.01, 0.21 ± 0.01, and 0.21 ± 0.01 mg/dl in creatinine; n = 5 in each group.). Moreover, no abnormality was observed at the injection site.

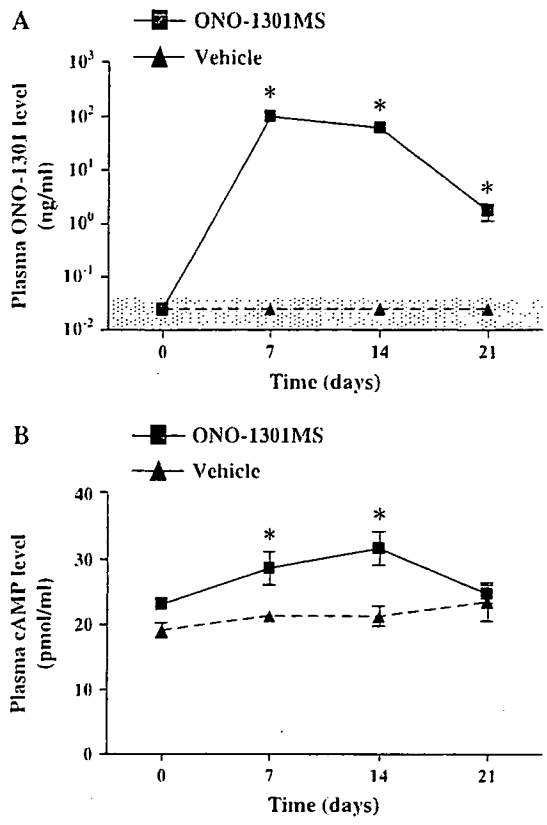


*Figure 3.* Time course changes in plasma ONO-1301 and cAMP. (*A*) Plasma ONO-1301 concentration after a single subcutaneous administration of ONO-1301MS or vehicle. The *shaded area* indicates below the lower limit of quantification (0.025 ng/ml) and is treated as 0 in the statistical analysis. (*B*) Changes in plasma cAMP level after a single subcutaneous administration of ONO-1301 MS or vehicle. Data are mean ± SEM. *$P < 0.05$ versus vehicle.

### Inhibitory Effect of ONO1301-MS on Proliferative Signals

To investigate the effect of ONO1301-MS on proliferative signals in the lung, Western blot analyses were performed. There were no significant differences in the expression of ERK1 and ERK2 among the three groups (Figure 7). However, phosphorylation of ERK1 and ERK2 was significantly increased in the control group, whereas these increases were markedly attenuated in the treatment group (Figure 7).

## DISCUSSION

In the present study, we demonstrated that (*1*) a novel sustained-release prostacyclin analog polymerized with PLGA

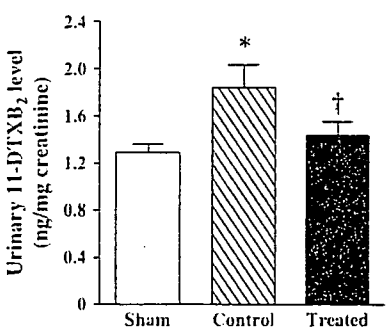


*Figure 4.* Effect of ONO-1301MS on thromboxane synthesis. Changes in urinary 11-dehydro thromboxane $B_2$ (11-DTX$B_2$) level on Day 14. Sham = sham rats given vehicle; control = monocrotaline (MCT)-treated rats given vehicle; treated = MCT rats treated with ONO-1301MS. Data are mean ± SEM. *$P <$ 0.05 versus sham; †$P <$ 0.05 versus control.

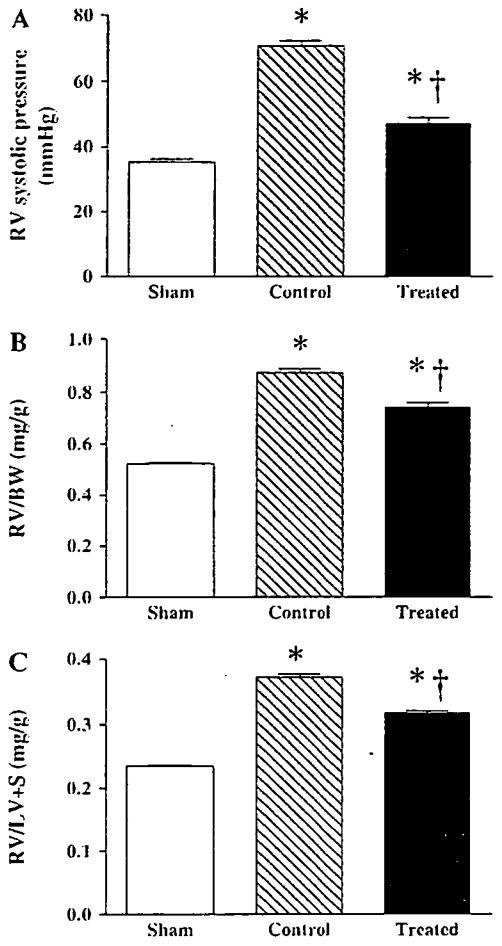


*Figure 5.* Effects of ONO-1301MS on pulmonary hemodynamics. (*A*) Effects of ONO-1301MS on right ventricular (RV) systolic pressure, (*B*) RV weight to body weight (RV/BW), and (C) RV weight to left ventricular plus septal weight (RV/LV + S). Sham = sham rats given vehicle; control = monocrotaline (MCT)-treated rats given vehicle; treated = MCT rats treated with ONO-1301MS. Data are mean ± SEM. $^*P < 0.05$ versus sham; $^\dagger P < 0.05$ versus control.

microspheres (ONO-1301MS) allowed a 3-week elevation of its circulating level, (2) ONO-1301MS had a sustained inhibitory effect on thromboxane synthase activity, and (*3*) a single subcutaneous administration of ONO-1301MS attenuated MCT-induced pulmonary hypertension in rats.

TABLE 1. PHYSIOLOGIC PROFILES OF THREE EXPERIMENTAL GROUPS

| | Sham* | Control† | Treated‡ |
|---|---|---|---|
| No. of rats | 10 | 11 | 11 |
| BW, g | 203 ± 4 | 165 ± 7§ | 175 ± 3§ |
| Heart rate, beats/min | 454 ± 7 | 441 ± 10 | 445 ± 6 |
| Mean arterial pressure, mm Hg | 110 ± 2 | 111 ± 3 | 107 ± 2 |
| LV + S/BW, mg/g | 2.23 ± 0.02 | 2.34 ± 0.02§ | 2.34 ± 0.04§ |

*Definition of abbreviations*: BW = body weight; LV = left ventricle; LV + S/BW = LV plus septal weight to body weight ratio.

Data are mean ± SEM. These measurements were performed on Day 21.

* Sham = rats given vehicle.

† Control = MCT rats given vehicle.

‡ Treated = MCT rats treated with ONO-1301MS.

§ $P < 0.05$ versus sham.

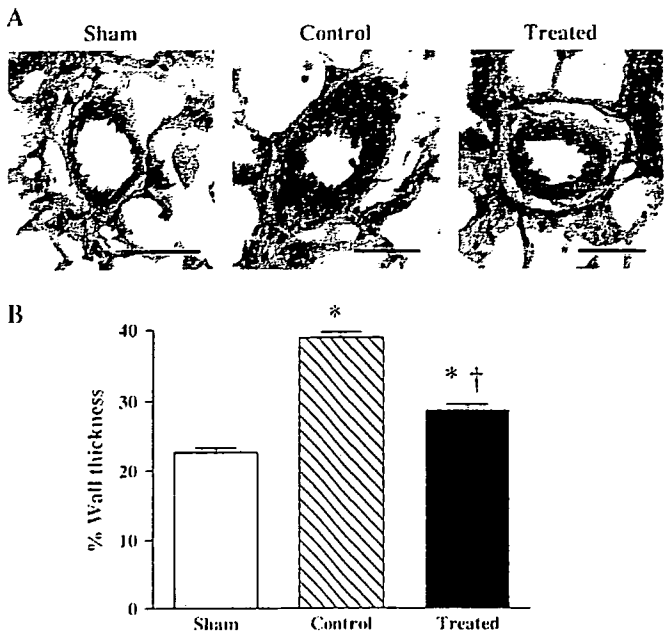


*Figure 6.* Effect of ONO-1301MS on vascular remodeling. (*A*) Representative photomicrographs of peripheral pulmonary arteries on Day 21. *Scale bars* = 50 μm. (*B*) Quantitative analysis of percentage of wall thickness in peripheral pulmonary arteries. Data are mean ± SEM. $^*P < 0.05$ versus sham; $^\dagger P < 0.05$ versus control.

Conventional prostacyclin and its analogs need continuous infusion or frequent administration because of their short duration of action. Previously, we reported a new type of prostacyclin agonist, ONO-1301, which has long-lasting prostacyclin activity and an inhibitory effect on thromboxane synthase (14). Although ONO-1301 has such interesting features, it still needs to be administered twice a day to achieve a significant improvement in pulmonary hypertension. To overcome this problem, we developed a new drug delivery system for prostacyclin. We polymerized ONO-1301 with PLGA microspheres to develop a novel sustained-release prostacyclin analog.

PLGA microspheres have been used as a controlled delivery system for bioactive agents (25). The release of bioactive agents from PLGA microspheres occurs through hydrolytic degradation of the polymeric matrix. Importantly, PLGA has already been used in humans. PLGA microspheres containing leuprorelin, a potent luteinizing hormone–releasing hormone analog, have been administered to patients with prostate and breast cancer by subcutaneous injection (26, 27). The rate of release of contents of PLGA microspheres can be changed by varying the factors affecting the hydrolytic degradation behavior of PLGA, such as lactate acid to glycolic acid ratio, average molecular weight of PLGA, and particle size (25). In the present study, we could control the degradation rate of ONO-1301MS. ONO-1301MS was designed to release ONO-1301 for 3 weeks, because it takes 3 weeks to induce pulmonary hypertension in rats after MCT injection. The present study demonstrated that the contained ONO-1301 was released for 3 weeks *in vitro*, producing a 3-week elevation of its circulating level after a single administration *in vivo*. It should be noted that only a single subcutaneous administration of ONO-1301MS attenuated MCT-induced pulmonary hypertension in rats. Thus, it might be possible to extend the administration interval for ONO-1301MS considerably longer than that with current prostacyclin analogs, and this could improve the quality of life in patients with pulmonary hypertension.

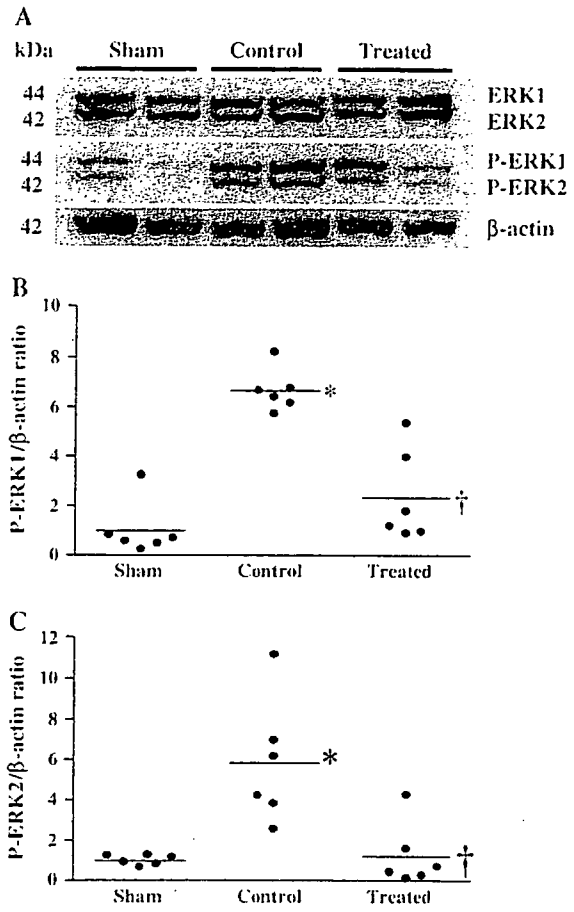


*Figure 7.* Effect of ONO-1301MS on extracellular signal-regulated protein kinase (ERK) phosphorylation. (*A*) Representative Western blotting for ERK, phospho-ERK (P-ERK) and β-actin (protein loading control) in lungs on Day 21 (n = 6 in each group). (*B* and *C*) Scatter plot of quantitative analysis of P-ERK expression in lung tissue. *Horizontal lines* in this figure show the mean value. $^{*}P < 0.05$ versus sham; $^{\dagger}P < 0.05$ versus control.

With regard to cAMP, which is a second messenger of prostacyclin and its analogs, it has been reported that plasma cAMP level remained increased after administration of prostacyclin analogs (23, 28). In our results, administration of ONO-1301MS increased the plasma cAMP level for over 2 weeks. This increase in plasma cAMP level was parallel to the change in plasma ONO-1301 level. In addition, ONO-1301MS attenuated the increase in urinary 11-$DTXB_2$ level in MCT rats 14 days after single administration. These results support that a single administration of ONO-1301MS produced a sustained beneficial effect for 3 weeks.

In the present study, we chose the maximum dose that did not induce significant hypotension. We did dose–response studies using ONO-1301MS (30, 100, and 300 mg/kg, respectively) (*see* Figure E1). ONO-1301MS at 300 mg/kg has induced significant hypotension. In addition, ONO-1301MS at 30 mg/kg did not significantly decrease RV systolic pressure (*see* Figure E3). On the other hand, ONO-1301MS at 100 mg/kg significantly decreased RV systolic pressure without significant hypotension. Furthermore, a single injection of 100 mg/kg ONO-1301 without PLGA or PLGA without ONO-1301 to MCT rats did not influence hemodynamics and vascular remodeling (*see* Figures E1–E3). These results suggest that a single injection of ONO-1301MS ameliorates MCT-induced pulmonary hypertension. Consistent with these hemodynamic data, RV/BW and medial wall thickness of pulmonary arteries, as indexes of RV hypertrophy and elevation of pulmonary arteriolar resistance, respectively, were significantly attenuated by the treatment with ONO-1301MS.

In histologic analysis, hypertrophy of pulmonary vessels after MCT injection was significantly attenuated by treatment with ONO-1301MS. An earlier clinical trial has shown that long-term therapy with epoprostenol significantly reduces pulmonary vascular resistance in patients who have no short-term response to vasodilators (5). It is speculated that such a beneficial effect of epoprostenol is caused not only by vasodilatation and antiplatelet aggregation but also by an antiproliferative effect on SMCs and reverse remodeling of pulmonary arteries. In the present study, phosphorylated ERK1/2 in the lung tissue was significantly increased after MCT injection. However, this increase was markedly attenuated by treatment with ONO-1301MS. ERK is the final component of the mitogen-activated protein kinase cascade. Prostacyclin has been shown to inhibit phosphorylation of ERK1/2 through the activation of cAMP (29). With respect to this signaling, protein kinase A (PKA), an intracellular effector of cAMP, has been shown to negatively regulate the Ras–ERK cascade by phosphorylating Raf and by preventing its association with active Ras (30). Furthermore, we previously reported that ONO-1301 inhibited pulmonary fibroblast proliferation through activation of the cAMP/PKA pathway (31). Therefore, it is interesting to speculate that ONO-1301MS may have antiproliferative effects on pulmonary vascular SMCs at least in part through inhibition of ERK via a cAMP-dependent pathway, although the precise mechanism remains to be elucidated.

ONO-1301MS significantly decreased urinary level of 11-$DTXB_2$, a metabolite of $TXA_2$. $TXA_2$ is a vasoconstrictor and a potent stimulator of platelet aggregation (32, 33). Moreover, it has been demonstrated that $TXA_2$ induces mitosis in vascular SMCs through activation of ERK (34, 35). It has been suggested that imbalance of thromboxane and prostacyclin plays an important role in the development of pulmonary hypertension (36). Previous reports showed that administration of thromboxane synthase inhibitor modestly attenuated pulmonary hypertension (37, 38). Thus, an inhibitory effect of ONO-1301MS on thromboxane synthase may also contribute to improvement in pulmonary hypertension.

In the present study, no adverse reactions, such as flushing, diarrhea, hypotension, renal dysfunction, or hepatic dysfunction, were observed in the treated group. However, further preclinical studies are necessary to confirm the safety and efficacy of ONO-1301MS before clinical trials start in patients with pulmonary arterial hypertension.

We did not measure cardiac output because of technical and mechanical problems. To support our hemodynamic data, we evaluated a variety of indexes, such as RV/BW and medial wall thickness of pulmonary arteries. These physiologic and histologic findings have been consistent with data on RV systolic pressure. Therefore, it is unlikely that the reduction in RV systolic pressure observed in the present study was related to the reduced cardiac output.

In conclusion, we developed a novel sustained-release prostacyclin analog polymerized with PLGA microspheres (ONO-1301MS), which achieved a 3-week elevation of its circulating level and simultaneously increased plasma cAMP levels for over 2 weeks, and had an inhibitory effect on thromboxane synthase. A single subcutaneous administration of ONO-1301MS attenuated MCT-induced pulmonary hypertension in rats. ONO-1301MS may have an antiproliferative effect through inhibition of ERK phosphorylation. This drug delivery system for a prostacyclin analog may be a new therapeutic strategy for the treatment of pulmonary arterial hypertension.

*Conflict of Interest Statement*: None of the authors has a financial relationship with a commercial entity that has an interest in the subject of this manuscript.

## References


1. McLaughlin VV, McGoon MD. Pulmonary arterial hypertension. *Circulation* 2006;114:1417–1431.
2. Moncada S, Gryglewski R, Bunting S, Vane JR. An enzyme isolated from arteries transforms prostaglandin endoperoxides to an unstable substance that inhibits platelet aggregation. *Nature* 1976;263:663–665.
3. Moncada S, Vane JR. Arachidonic acid metabolites and the interactions between platelets and blood-vessel walls. *N Engl J Med* 1979;300: 1142–1147.
4. Humbert M, Sitbon O, Simonneau G. Treatment of pulmonary arterial hypertension. *N Engl J Med* 2004;351:1425–1436.
5. McLaughlin VV, Genthner DE, Panella MM, Rich S. Reduction in pulmonary vascular resistance with long-term epoprostenol (prostacyclin) therapy in primary pulmonary hypertension. *N Engl J Med* 1998;338:273–277.
6. McLaughlin VV, Shillington A, Rich S. Survival in primary pulmonary hypertension: the impact of epoprostenol therapy. *Circulation* 2002; 106:1477–1482.
7. Sitbon O, Humbert M, Nunes H, Parent F, Garcia G, Herve P, Rainisio M, Simonneau G. Long-term intravenous epoprostenol infusion in primary pulmonary hypertension: prognostic factors and survival. *J Am Coll Cardiol* 2002;40:780–788.
8. Okano Y, Yoshioka T, Shimouchi A, Satoh T, Kunieda T. Orally active prostacyclin analogue in primary pulmonary hypertension. *Lancet* 1997;349:1365.
9. Nagaya N, Uematsu M, Okano Y, Satoh T, Kyotani S, Sakamaki F, Nakanishi N, Miyatake K, Kunieda T. Effect of orally active prostacyclin analogue on survival of outpatients with primary pulmonary hypertension. *J Am Coll Cardiol* 1999;34:1188–1192.
10. Olschewski H, Simonneau G, Galie N, Higenbottam T, Naeije R, Rubin LJ, Nikkho S, Speich R, Hoeper MM, Behr J, *et al.* Inhaled iloprost for severe pulmonary hypertension. *N Engl J Med* 2002;347:322–329.
11. Simonneau G, Barst RJ, Galie N, Naeije R, Rich S, Bourge RC, Keogh A, Oudiz R, Frost A, Blackburn SD, *et al.* Continuous subcutaneous infusion of treprostinil, a prostacyclin analogue, in patients with pulmonary arterial hypertension: a double-blind, randomized, placebo-controlled trial. *Am J Respir Crit Care Med* 2002;165:800–804.
12. Badesch DB, McLaughlin VV, Delcroix M, Vizza CD, Olschewski H, Sitbon O, Barst RJ. Prostanoid therapy for pulmonary arterial hypertension. *J Am Coll Cardiol* 2004;43:56S–61S.
13. Laliberte K, Arneson C, Jeffs R, Hunt T, Wade M. Pharmacokinetics and steady-state bioequivalence of treprostinil sodium (Remodulin) administered by the intravenous and subcutaneous route to normal volunteers. *J Cardiovasc Pharmacol* 2004;44:209–214.
14. Kataoka M, Nagaya N, Satoh T, Itoh T, Murakami S, Iwase T, Miyahara Y, Kyotani S, Sakai Y, Kangawa K, *et al.* A long-acting prostacyclin agonist with thromboxane inhibitory activity for pulmonary hypertension. *Am J Respir Crit Care Med* 2005;172:1575–1580.
15. Alonso MJ, Gupta RK, Min C, Siber GR, Langer R. Biodegradable microspheres as controlled-release tetanus toxoid delivery systems. *Vaccine* 1994;12:299–306.
16. Seagal J, Edry E, Keren Z, Leider N, Benny O, Machluf M, Melamed D. A fail-safe mechanism for negative selection of isotype-switched B cell precursors is regulated by the Fas/FasL pathway. *J Exp Med* 2003;198:1609–1619.
17. Mullerad J, Cohen S, Benharroch D, Apte RN. Local delivery of IL-1 alpha polymeric microspheres for the immunotherapy of an experimental fibrosarcoma. *Cancer Invest* 2003;21:720–728.
18. Mullerad J, Cohen S, Voronov E, Apte RN. Macrophage activation for the production of immunostimulatory cytokines by delivering interleukin 1 via biodegradable microspheres. *Cytokine* 2000;12:1683–1690.
19. Sanchez A, Gupta RK, Alonso MJ, Siber GR, Langer R. Pulsed controlled-released system for potential use in vaccine delivery. *J Pharm Sci* 1996;85:547–552.
20. Roullin VG, Lemaire L, Venier-Julienne MC, Faisant N, Franconi F, Benoit JP. Release kinetics of 5-fluorouracil-loaded microspheres on an experimental rat glioma. *Anticancer Res* 2003;23:21–25.
21. Kimura H, Kasahara Y, Kurosu K, Sugito K, Takiguchi Y, Terai M, Mikata A, Natsume M, Mukaida N, Matsushima K, *et al.* Alleviation of monocrotaline-induced pulmonary hypertension by antibodies to monocyte chemotactic and activating factor/monocyte chemoattractant protein-1. *Lab Invest* 1998;78:571–581.
22. Ono S, Voelkel NF. PAF antagonists inhibit monocrotaline-induced lung injury and pulmonary hypertension. *J Appl Physiol* 1991;71:2483–2492.
23. Itoh T, Nagaya N, Fujii T, Iwase T, Nakanishi N, Hamada K, Kangawa K, Kimura H. A combination of oral sildenafil and beraprost ameliorates pulmonary hypertension in rats. *Am J Respir Crit Care Med* 2004;169:34–38.
24. Fiorucci S, Mencarelli A, Meneguzzi A, Lechi A, Morelli A, del Soldato P, Minuz P. NCX-4016 (NO-aspirin) inhibits lipopolysaccharide-induced tissue factor expression in vivo: role of nitric oxide. *Circulation* 2002;106:3120–3125.
25. Shive MS, Anderson JM. Biodegradation and biocompatibility of PLA and PLGA microspheres. *Adv Drug Deliv Rev* 1997;28:5–24.
26. Fornara P, Jocham D. Clinical study results of the new formulation leuprorelin acetate three-month depot for the treatment of advanced prostate carcinoma. *Urol Int* 1996;56:18–22.
27. Schmid P, Untch M, Kosse V, Bondar G, Vassiljev L, Tarutinov V, Lehmann U, Maubach L, Meurer J, Wallwiener D, *et al.* Leuprorelin acetate every-3-months depot versus cyclophosphamide, methotrexate, and fluorouracil as adjuvant treatment in premenopausal patients with node-positive breast cancer: the TABLE study. *J Clin Oncol* 2007;25:2509–2515.
28. Beghetti M, Reber G, de Moerloose P, Vadas L, Chiappe A, Spahr-Schopfer I, Rimensberger PC. Aerosolized iloprost induces a mild but sustained inhibition of platelet aggregation. *Eur Respir J* 2002; 19:518–524.
29. Li RC, Cindrova-Davies T, Skepper JN, Sellers LA. Prostacyclin induces apoptosis of vascular smooth muscle cells by a cAMP-mediated inhibition of extracellular signal-regulated kinase activity and can counteract the mitogenic activity of endothelin-1 or basic fibroblast growth factor. *Circ Res* 2004;94:759–767.
30. Cook SJ, McCormick F. Inhibition by cAMP of Ras-dependent activation of Raf. *Science* 1993;262:1069–1072.
31. Murakami S, Nagaya N, Itoh T, Kataoka M, Iwase T, Horio T, Miyahara Y, Sakai Y, Kangawa K, Kimura H. Prostacyclin agonist with thromboxane synthase inhibitory activity (ONO-1301) attenuates bleomycin-induced pulmonary fibrosis in mice. *Am J Physiol Lung Cell Mol Physiol* 2006;290:L59–L65.
32. Hamberg M, Svensson J, Samuelsson B. Prostaglandin endoperoxides: a new concept concerning the mode of action and release of prostaglandins. *Proc Natl Acad Sci USA* 1974;71:3824–3828.
33. Svenssen J, Strandberg K, Tuvemo T, Hamberg M. Thromboxane A2: effects on airway and vascular smooth muscle. *Prostaglandins* 1977; 14:425–436.
34. Sachinidis A, Flesch M, Ko Y, Schror K, Bohm M, Dusing R, Vetter H. Thromboxane A2 and vascular smooth muscle cell proliferation. *Hypertension* 1995;26:771–780.
35. Morinelli TA, Tempel GE, Jaffa AA, Silva RH, Naka M, Folger W, Halushka PV. Thromboxane A2/prostaglandin H2 receptors in streptozotocin-induced diabetes: effects of insulin therapy in the rat. *Prostaglandins* 1993;45:427–438.
36. Christman BW, McPherson CD, Newman JH, King GA, Bernard GR, Groves BM, Loyd JE. An imbalance between the excretion of thromboxane and prostacyclin metabolites in pulmonary hypertension. *N Engl J Med* 1992;327:70–75.
37. Nagata T, Uehara Y, Hara K, Igarashi K, Hazama H, Hisada T, Kimura K, Goto A, Omata M. Thromboxane inhibition and monocrotaline-induced pulmonary hypertension in rats. *Respirology* 1997;2:283–289.
38. Rich S, Hart K, Kieras K, Brundage BH. Thromboxane synthetase inhibition in primary pulmonary hypertension. *Chest* 1987;91:356–360.

*Am J Physiol Heart Circ Physiol* 294: H441–H448, 2008.
First published November 16, 2007; doi:10.1152/ajpheart.01021.2007.

# Role of Cu,Zn-SOD in the synthesis of endogenous vasodilator hydrogen peroxide during reactive hyperemia in mouse mesenteric microcirculation in vivo

**Toyotaka Yada,[1] Hiroaki Shimokawa,[2] Keiko Morikawa,[3] Aya Takaki,[2] Yoshiro Shinozaki,[4] Hidezo Mori,[5] Masami Goto,[1] Yasuo Ogasawara,[1] and Fumihiko Kajiya[1]**

[1]*Department of Medical Engineering and Systems Cardiology, Kawasaki Medical School, Kurashiki, Japan;* [2]*Department of Cardiovascular Medicine, Tohoku University Graduate School of Medicine, Sendai, Japan;* [3]*Department of Anesthesiology, Kyushu University Graduate School of Medical Sciences, Fukuoka, Japan;* [4]*Department of Physiology, Tokai University School of Medicine, Isehara, Japan; and* [5]*Department of Cardiac Physiology, National Cardiovascular Center Research Institute, Suita, Japan*

Submitted 4 September 2007; accepted in final form 12 November 2007

**Yada T, Shimokawa H, Morikawa K, Takaki A, Shinozaki Y, Mori H, Goto M, Ogasawara Y, Kajiya F.** Role of Cu,Zn-SOD in the synthesis of endogenous vasodilator hydrogen peroxide during reactive hyperemia in mouse mesenteric microcirculation in vivo. *Am J Physiol Heart Circ Physiol* 294: H441–H448, 2008. First published November 16, 2007; doi:10.1152/ajpheart.01021.2007.—We have recently demonstrated that endothelium-derived hydrogen peroxide ($H_2O_2$) is an endothelium-derived hyperpolarizing factor and that endothelial Cu/Zn-superoxide dismutase (SOD) plays an important role in the synthesis of endogenous $H_2O_2$ in both animals and humans. We examined whether SOD plays a role in the synthesis of endogenous $H_2O_2$ during in vivo reactive hyperemia (RH), an important regulatory mechanism. Mesenteric arterioles from wild-type and Cu,Zn-SOD$^{-/-}$ mice were continuously observed by a pencil-type charge-coupled device (CCD) intravital microscope during RH (reperfusion after 20 and 60 s of mesenteric artery occlusion) in the cyclooxygenase blockade under the following four conditions: control, catalase alone, $N^G$-monomethyl-L-arginine (L-NMMA) alone, and L-NMMA + catalase. Vasodilatation during RH was significantly decreased by catalase or L-NMMA alone and was almost completely inhibited by L-NMMA + catalase in wild-type mice, whereas it was inhibited by L-NMMA and L-NMMA + catalase in the Cu,Zn-SOD$^{-/-}$ mice. RH-induced increase in blood flow after L-NMMA was significantly increased in the wild-type mice, whereas it was significantly reduced in the Cu,Zn-SOD$^{-/-}$ mice. In mesenteric arterioles of the Cu,Zn-SOD$^{-/-}$ mice, Tempol, an SOD mimetic, significantly increased the ACh-induced vasodilatation, and the enhancing effect of Tempol was decreased by catalase. Vascular $H_2O_2$ production by fluorescent microscopy in mesenteric arterioles after RH was significantly increased in response to ACh in wild-type mice but markedly impaired in Cu,Zn-SOD$^{-/-}$ mice. Endothelial Cu,Zn-SOD plays an important role in the synthesis of endogenous $H_2O_2$ that contributes to RH in mouse mesenteric smaller arterioles.

nitric oxide; endothelium-derived hyperpolarizing factor; arteriole; vasodilatation

THE ENDOTHELIUM SYNTHESIZES and releases endothelium-derived relaxing factors (EDRFs), including vasodilator prostaglandins, nitric oxide (NO), and as yet unidentified endothelium-derived hyperpolarizing factor (EDHF). Since the first reports on the existence of EDHFs (4, 8), several candidates for EDHF have been proposed (9), including cytochrome *P*-450 metabolites (2, 3), endothelium-derived $K^+$ channel (7), and electrical communications through gap junctions between endothelial cells and vascular smooth muscle cells (34). Matoba et al. (19a, 19b, 20) previously identified that endothelium-derived hydrogen peroxide ($H_2O_2$) is a primary EDHF in mesenteric arteries of mice, pigs, and humans. Morikawa et al. (24a, 25) subsequently confirmed that endothelial Cu/Zn-superoxide dismutase (SOD) plays an important role in synthesizing EDHF/$H_2O_2$ in mice and humans. Recently, our laboratory (41a, 42) confirmed that endogenous $H_2O_2$ plays an important role for autoregulation and protection against reperfusion injury in canine coronary microcirculation.

Reactive hyperemia (RH) is an important regulatory mechanism of the cardiovascular system in response to a temporal reduction in blood flow for which both mechanosensitive (e.g., myogenic and shear mediated) and metabolic regulatory processes may be involved (6, 14a, 28). For the RH response of canine coronary microcirculation, NO, ATP-sensitive $K^+$ channels, and adenosine may all be involved (11, 41). Shear stress plays a crucial role in modulating vascular tone by stimulating the release of EDRFs (8, 32), and all three EDRFs ($PGI_2$, NO, and EDHF) are involved in flow-induced vasodilatation (15, 18, 33, 44).

However, it remains to be examined whether endogenous $H_2O_2$ is involved in the vasodilator mechanism of RH and, if so, whether endothelial Cu,Zn-SOD plays a role in the synthesis of endogenous $H_2O_2$ during RH. The present study was thus designed to address these important issues in mice. Our laboratory (42, 44) previously reported that the contribution of EDHF to the vasodilatory mechanisms increases as the diameter of the vessel decreases. Thus, by employing a pencil-type charge-coupled device (CCD) intravital microscope with a high resolution, we focused on the arterioles with a diameter of $<50$ μm in vivo.

## METHODS

The present study was approved by the Animal Care and Use Committee of Kawasaki Medical School and conformed to the guidelines on animal experiments of Kawasaki Medical School and *the*

Address for reprint requests and other correspondence: Toyotaka Yada, Dept. of Medical Engineering and Systems Cardiology, Kawasaki Medical School, 577 Matsushima, Kurashiki, Okayama 701-0192 Japan (e-mail: yada@me.kawasaki-m.ac.jp).

The costs of publication of this article were defrayed in part by the payment of page charges. The article must therefore be hereby marked "*advertisement*" in accordance with 18 U.S.C. Section 1734 solely to indicate this fact.

*Guide for the Care and Use of Laboratory Animals* published by the National Institutes of Health.

*Animal preparation.* Male Cu,Zn-SOD$^{-/-}$ and control mice (10–16 wk of age) derived from breeding pairs of heterozygous (Cu,Zn-SOD$^{+/-}$) mice (Jackson Laboratory, Bar Harbor, ME) were used (25). They were placed on a heating blanket to maintain body temperature at 37°C throughout the experiment. The animals were anesthetized with 1% inhalational anesthesia of isoflurane. After tracheal intubation, they were ventilated with a mixture of room air and oxygen by a ventilator. The abdomen was opened, and a 24-Fr catheter was inserted into the abdominal aorta to measure aortic pressure. Mesenteric arterioles were continuously observed by a pencil-type intravital microscope (Nihon Kohden, Tokyo, Japan) (13).

*Measurements of diameter by pencil-type intravital microscope.* Mesenteric arterioles were visualized using a pencil-type intravital microscope (13). The system was modified for the visualization of microcirculation from our previous needle-probe CCD videomicroscope system (40). The microscopic images were monitored and recorded on a digital videocassette recorder (Sony, Tokyo, Japan) every 33 ms (30 frames/s). The spatial resolution of a static image of this system is 0.5 μm for ×600 magnification. The field of view is 367 × 248 μm, and the focal depth is 50 μm.

*Measurements of regional blood flow in mesenteric arteries.* Regional blood flow in mesenteric arteries was measured by the nonradioactive microsphere (15 μm; Sekisui Plastic, Tokyo, Japan) technique at the end of the experiments, as previously described (24). Briefly, a bolus (50 μl) of the microspheres suspension (5 × $10^5$ spheres; Ce and Ba) were injected into the abdominal aorta at baseline and 5 s after the reperfusion of the mesenteric artery with confirming changes of the blood flow of the mesenteric artery by a CCD intravital microscope and without inducing hemodynamic changes (14). Mice were euthanized, and the mesenterium was extracted. The X-ray fluorescence of the stable heavy elements was measured by a wavelength-dispersive spectrometer (model PW 1480; Phillips, Eindhoven, the Netherlands). The relative increase in blood flow of mesenterium [microsphere count/tissue weight (g)] during RH from baseline was calculated.

*Detection of $H_2O_2$ and NO production in mesenteric microvessels.* 2′,7′-Dichlorodihydrofluorescein diacetate (DCF-DA; Molecular Probes, Eugene, OR) and diaminorhodamine-4M AM (DAR; Daiichi Pure Chemicals, Tokyo, Japan) were used to detect $H_2O_2$ and NO production in mesenteric microvessels, respectively, as previously described (41a). Briefly, fresh and unfixed mesenteric tissue was cut into several blocks and immediately frozen in an optimal cutting temperature compound (Tissue-Tek; Sakura Fine Chemical, Tokyo, Japan). After washout of the mesenteric tissue with phosphate-buffered solution under a normal temperature, fluorescent images of the microvessels were obtained 3 min after application of acetylcholine (ACh) by using a fluorescence microscope (Olympus BX51) (41a). We defined the baseline fluorescent intensity as the response in the vascular endothelium just after the injection of NO or $H_2O_2$ fluorescent dye. The fluorescence data at baseline (both DCF-DA and DAR) were obtained after the RH.

*Experimental protocol.* We performed four protocols. First, mesenteric arterioles in wild-type and Cu,Zn-SOD$^{-/-}$ mice were continuously observed by a pencil-type intravital microscope during RH (reperfusion after 20 and 60 s of mesenteric artery occlusion) with cyclooxygenase blockade [indomethacin, 5 × $10^{-5}$ mol/l topical administration (ta)] with the following four conditions: control, catalase alone [1,500 U·min$^{-1}$·100 g body wt$^{-1}$ intra-arterial administration (ia) polyethylene glycol-catalase, a specific decomposer of $H_2O_2$], NO synthase inhibitor alone ($10^{-4}$ mol/l ta L-NMMA), and L-NMMA + catalase (17). In the presence of indomethacin and L-NMMA, microspheres were administered at baseline and 5 s after the reperfusion into the abdominal aorta by bolus injection because RH peaked within 20–60 s after release from 20- and 60-s occlusion (29). Maximal vascular diameter was measured within 20 and 60 s after the reperfusion. Second, ACh ($10^{-7}$ to $10^{-5}$ mol/l ta)-induced endothelium-dependent vasodilatation was examined under the control conditions and in the presence of Tempol, a SOD mimetic 4-hydroxy-2,2,6,6-tetramethylpiperidine-*N*-oxyl (50 μg·min$^{-1}$·100 g body wt$^{-1}$ ia) (17), and Tempol + catalase. In the combined infusion protocol (Tempol or Tempol + catalase) in the presence of cyclooxygenase blockade + L-NMMA, the combined infusion was performed simultaneously for 20 min, ACh was infused for 10 min, and the vascular diameter was measured. Third, sodium nitroprusside (SNP; $10^{-7}$ to $10^{-5}$ mol/l ta, each 10 min)-induced endothelium-independent vasodilatation was examined in wild-type and Cu,Zn-SOD$^{-/-}$ mice. Fourth, fresh and unfixed mesenteric tissue was then cut into several blocks and immediately frozen in optimal cutting temperature compound.

*Statistical analysis.* The results are expressed as means ± SE. Dose-response curves were analyzed by two-way ANOVA followed by the Scheffé's post hoc test for multiple comparisons. Vascular responses were analyzed by one-way ANOVA followed by the Scheffé's post hoc test for multiple comparisons. $P < 0.05$ was considered to be statistically significant.

## RESULTS

*Hemodynamics and blood gases during RH.* Throughout the experiments, mean aortic pressure and heart rate were constant and comparable (Tables 1 and 2), and $Po_2$, $Pco_2$, and pH were maintained within the physiological ranges (>70 mmHg $Po_2$, 25–40 mmHg $Pco_2$, and pH 7.35–7.45). Baseline mesenteric

Table 1. *Hemodynamics during RH*

| | | Control | | Catalase | | L-NMMA | | L-NMMA + Catalase | |
|---|---|---|---|---|---|---|---|---|---|
| | *n* | B | RH | B | RH | B | RH | B | RH |
| MBP, RH 20, mmHg | | | | | | | | | |
| WT | 10 | 83±7 | 85±9 | 81±7 | 82±7 | 82±8 | 81±6 | 83±8 | 82±6 |
| Cu/Zn-SOD$^{-/-}$ | 10 | 85±12 | 87±10 | 83±8 | 82±8 | 82±8 | 82±8 | 82±8 | 80±9 |
| MBP, RH 60, mmHg | | | | | | | | | |
| WT | 5 | 86±8 | 88±7 | 87±7 | 88±7 | 88±8 | 87±7 | 88±7 | 87±7 |
| Cu/Zn-SOD$^{-/-}$ | 5 | 88±8 | 86±8 | 87±6 | 89±9 | 88±7 | 88±8 | 89±6 | 90±11 |
| HR, RH 20, beats/min | | | | | | | | | |
| WT | 10 | 346±14 | 348±14 | 335±15 | 333±17 | 315±15 | 310±17 | 330±18 | 330±18 |
| Cu/Zn-SOD$^{-/-}$ | 10 | 364±27 | 354±22 | 350±18 | 351±15 | 355±15 | 340±17 | 355±15 | 335±17 |
| HR, RH 60, beats/min | | | | | | | | | |
| WT | 5 | 351±31 | 361±9 | 353±21 | 356±13 | 358±10 | 364±37 | 354±22 | 355±15 |
| Cu/Zn-SOD$^{-/-}$ | 5 | 346±18 | 356±25 | 356±15 | 361±19 | 351±31 | 361±9 | 358±10 | 364±27 |

Values are means ± SE; *n*, number of rats. RH, reactive hyperemia; L-NMMA, $N^G$-monomethyl-L-arginine; B, baseline; MBP, mean blood pressure; HR, heart rate; WT, wild-type.

Table 2. *Hemodynamics during administration of ACh and SNP*

| | | Control | | | | Tempol | | | Tempol + Catalase | | | SNP | | | |
|---|---|---|---|---|---|---|---|---|---|---|---|---|---|---|---|
| | $n$ | B | ACh $10^{-7}$ | ACh $10^{-6}$ | ACh $10^{-5}$ | ACh $10^{-7}$ | ACh $10^{-6}$ | ACh $10^{-5}$ | ACh $10^{-7}$ | ACh $10^{-6}$ | ACh $10^{-5}$ | B | SNP $10^{-7}$ | SNP $10^{-6}$ | SNP $10^{-5}$ |
| MBP, mmHg | | | | | | | | | | | | | | | |
| WT | 10 | 90±7 | 88±7 | 87±7 | 89±6 | 91±10 | 90±11 | 84±11 | 91±8 | 86±8 | 86±8 | 78±13 | 77±13 | 76±13 | 76±13 |
| Cu/Zn-SOD$^{-/-}$ | 10 | 93±11 | 92±10 | 94±10 | 97±10 | 98±16 | 97±15 | 99±15 | 91±8 | 91±8 | 88±8 | 81±8 | 77±10 | 75±11 | 74±11 |
| HR, beats/min | | | | | | | | | | | | | | | |
| WT | 10 | 361±9 | 340±17 | 340±17 | 340±17 | 342±24 | 336±25 | 336±25 | 320±19 | 330±27 | 330±27 | 370±57 | 364±37 | 351±31 | 351±31 |
| Cu/Zn-SOD$^{-/-}$ | 10 | 386±11 | 381±24 | 371±21 | 396±13 | 386±11 | 377±15 | 377±15 | 362±22 | 356±25 | 356±25 | 372±21 | 369±6 | 358±10 | 346±18 |

Values are means ± SE; $n$, number of rats. SNP, sodium nitroprusside; ACh, acetylcholine.

arteriolar diameter was comparable in the absence and presence of inhibitors under the four different experimental conditions (Tables 3 and 4). Those different inhibitors (L-NMMA, catalase, and Tempol) did not affect basal diameter.

*Mesenteric vasodilatation during RH.* We were able to observe EDHF-sensitive smaller arterioles (18–66 μm) by using a newly developed pencil-type CCD intravital microscope with a higher resolution. In the mesenteric arterioles of wild-type mice, vasodilatation during RH to 20- and 60-s arterial occlusion was decreased by catalase or L-NMMA alone and was almost completely inhibited by L-NMMA + catalase (Fig. 1). In contrast, in mesenteric arterioles of Cu,Zn-SOD$^{-/-}$ mice, vasodilatation during RH to 20- and 60-s arterial occlusion was decreased by catalase alone and was almost completely inhibited by L-NMMA alone or L-NMMA + catalase (Fig. 1). Blood flow measurement by microsphere technique showed that in the presence of indomethacin and L-NMMA, RH-induced increase in blood flow was 232 ± 4% (20 s) and 331 ± 4% (60 s) of baseline in control and was sensitive to catalase (137 ± 4%, 20 s; and 147 ± 17%, 60 s) in the wild-type mice, whereas in the Cu,Zn-SOD$^{-/-}$ mice, the vasodilator response was significantly reduced to 125 ± 19% (20 s) and 145 ± 23% (60 s) in control and was insensitive to catalase (120 ± 24%, 20 s; and 139 ± 19%, 60 s) (Fig. 2). With the longer occlusion of the mesenteric artery, the shear stimulus for $H_2O_2$ release was significantly increased in the control condition and was significantly decreased by catalase.

*Endothelium-dependent vasodilatation.* In mesenteric arterioles of wild-type mice, endothelium-dependent vasodilatation to ACh ($10^{-7}$ to $10^{-5}$ mol/l in the presence of indomethacin and L-NMMA) was unchanged with Tempol but significantly inhibited by the addition of catalase (Fig. 3). In contrast, in the mesenteric arterioles of the Cu,Zn-SOD$^{-/-}$ mice, the response to ACh was significantly enhanced with Tempol, a response that was sensitive to the addition of catalase (Fig. 3).

*Endothelium-independent vasodilatation.* Endothelium-independent vasodilatation to SNP ($10^{-7}$ to $10^{-5}$ mol/l in the presence of L-NMMA + catalase) was comparable between the two strains (Table 4).

*Detection of $H_2O_2$ and NO production in the mesenteric artery.* Fluorescent microscopy with DCF-DA showed that vascular $H_2O_2$ production in mesenteric arterioles was significantly increased in response to ACh in wild-type mice compared with baseline but markedly impaired in Cu,Zn-SOD$^{-/-}$ mice (Fig. 4). In contrast, vascular NO production in mesenteric arterioles, as assessed by DAR fluorescent intensity, was significantly increased in response to ACh in wild-type mice compared with baseline and was unaltered in Cu,Zn-SOD$^{-/-}$ mice (Fig. 5).

## DISCUSSION

The novel finding of the present study with a newly developed pencil-type CCD intravital microscope in vivo is that Cu,Zn-SOD plays an important role in the synthesis of endogenous $H_2O_2$, which is substantially involved in the mechanisms of RH-induced vasodilatation in mouse mesenteric circulation.

*Impaired EDHF-mediated vasodilatation in Cu,Zn-SOD$^{-/-}$ mice in vivo.* Matoba et al. (19a, 20) have previously identified that endothelium-derived $H_2O_2$ is an EDHF in mouse and

Table 3. *Diameter change during RH*

| | Control | | Catalase | | L-NMMA | | L-NMMA + Catalase | |
|---|---|---|---|---|---|---|---|---|
| | B | RH | B | RH | B | RH | B | RH |
| RH 20, μm | | | | | | | | |
| WT | 36±4 | 49±4† | 36±4 | 44±4† | 36±3 | 42±3* | 36±4 | 38±3 |
| Cu/Zn-SOD$^{-/-}$ | 36±4 | 48±5† | 36±4 | 42±5† | 36±4 | 38±4 | 36±3 | 38±4 |
| RH 60, μm | | | | | | | | |
| WT | 40±4 | 55±4† | 40±4 | 51±4† | 40±5 | 47±4* | 39±4 | 41±4 |
| Cu/Zn-SOD$^{-/-}$ | 40±3 | 56±4† | 40±3 | 51±4† | 39±4 | 42±3 | 40±5 | 42±3 |

Values are means ± SE; *n*, number of arterioles per animal. *$P$ < 0.01 vs. B.

human mesenteric microvessels. Subsequently, our laboratory (42) and others (23) have confirmed that endogenous $H_2O_2$ exerts important vasodilator effects in canine coronary microcirculation in vivo and in isolated human coronary microvessels, respectively. $H_2O_2$ can be formed from superoxide anions derived from several sources in endothelial cells, including endothelial NO synthase (eNOS), cyclooxygenase, lipoxygenase, cytochrome *P*-450 enzymes, and reduced NADP [NAD(P)H] oxidases. Gupte et al. (10) demonstrated that cytosolic NADH redox and Cu,Zn-SOD activity have important roles in controlling the inhibitory effects of superoxide anions derived from NADH oxidase. Morikawa et al. (24a, 25) have also demonstrated that endothelial Cu,Zn-SOD plays an important role in the synthesis of $H_2O_2$ in mouse and human mesenteric arteries in vitro.

In the present study, catalase or L-NMMA alone significantly, but not completely, inhibited the RH-induced vasodilatation of mesenteric arterioles in wild-type mice in vivo, whereas L-NMMA + catalase markedly attenuated the remaining vasodilatation. In contrast, in Cu,Zn-SOD$^{-/-}$ mice, L-NMMA alone significantly decreased the vasodilatation and blood flow in response to 20- and 60-s arterial occlusion (Figs. 1 and 2). These results obtained using a pencil-type CCD intravital microscope indicate that $H_2O_2$ exerts important vasodilator effects on mesenteric smaller arterioles during RH and that Cu,Zn-SOD plays an important role in the synthesis of endogenous $H_2O_2$ during RH in vivo. Koller and Bagi (14a) showed that RH in rat isolated coronary arterioles was sensitive to pressure/stretch and flow/shear stress. Miura et al. (23) also showed the important role of endogenous $H_2O_2$ in flow-induced vasodilatation of human coronary arterioles. Koller and Bagi (14a) also suggested that $H_2O_2$ contributes to the development of the early peak phase of RH but not the duration of reactive vasodilatation, whereas NO prolongs the later phase of RH in rat isolated coronary arterioles, suggesting that $H_2O_2$ released endogenously within the vascular wall changes hemodynamic forces. In the present study, peak blood flow was significantly decreased after catalase (Fig. 2), suggesting that flow-induced vasodilatation during the early phase of RH is indeed mediated by $H_2O_2$ in mouse mesenteric arterioles in vivo.

*Compensatory vasodilator mechanism between $H_2O_2$ and NO.* It is well known that coronary vascular tone is regulated by the interactions among hemodynamic forces and several endogenous vasodilators, including NO, $H_2O_2$, and adenosine (41a, 42). Koller and Bagi (14a) demonstrated that mechanosensitive mechanisms were activated by changes in pressure and flow/shear stress during RH in isolated coronary arterioles. A superoxide anion is dismutated to $H_2O_2$ by manganese SOD (Mn-SOD, mitochondrial matrix) and Cu,Zn-SOD. $H_2O_2$ diffuses across the mitochondrial membrane to act on vascular smooth muscle (45). Tsunoda et al. (35) demonstrated that Mn-SOD augmented RH during 60-s canine coronary ischemia and reperfusion. $H_2O_2$ generated in the arteriolar smooth muscle could cause the response of activation of cGMP in rat skeletal muscle arterioles (38). Kitakaze et al. (12) indicated that the augmentation of reactive hyperemic flow caused by SOD is attributed to the enhanced release of adenosine in canine coronary circulation. These endogenous vasodilators may play an important role in causing the compensatory vasodilatation of coronary microvessels during myocardial ischemia.

In the present study, endothelium-dependent vasodilatation during RH (in the presence of L-NMMA) was almost completely inhibited by catalase in wild-type mice. In the Cu,Zn-SOD$^{-/-}$ mice, vasodilatation during RH remained under the control condition but was almost completely inhibited by L-NMMA (Fig. 1). The RH-induced increase in blood flow (in the presence of indomethacin and L-NMMA) was significantly inhibited by catalase in the wild-type mice but not in Cu,Zn-SOD$^{-/-}$ mice (Fig. 2). RH-induced increase in blood flow (in the presence of indomethacin and L-NMMA) remained in Cu,Zn-SOD$^{-/-}$ mice (Fig. 2). $H_2O_2$ may compensate for the loss of action of NO. $H_2O_2$ produced by SOD other than Cu,Zn-SOD may compensate for the loss of action of Cu,Zn-SOD-derived $H_2O_2$.

Table 4. *Diameter change during administration of ACh and SNP*

| | ACh | | | | SNP | | | |
|---|---|---|---|---|---|---|---|---|
| | B | ACh $10^{-7}$ | ACh $10^{-6}$ | ACh $10^{-5}$ | B | SNP $10^{-7}$ | SNP $10^{-6}$ | SNP $10^{-5}$ |
| WT, μm | 36±3 | 41±3* | 45±3† | 49±4† | 35±4 | 39±4* | 43±5† | 46±5† |
| Cu/Zn-SOD$^{-/-}$, μm | 36±4 | 38±4 | 41±4* | 44±4† | 34±4 | 38±4* | 41±4† | 44±4† |

Values are means ± SE; *n*, number of arterioles per animal. *$P$ < 0.05; †$P$ < 0.01 vs. B.

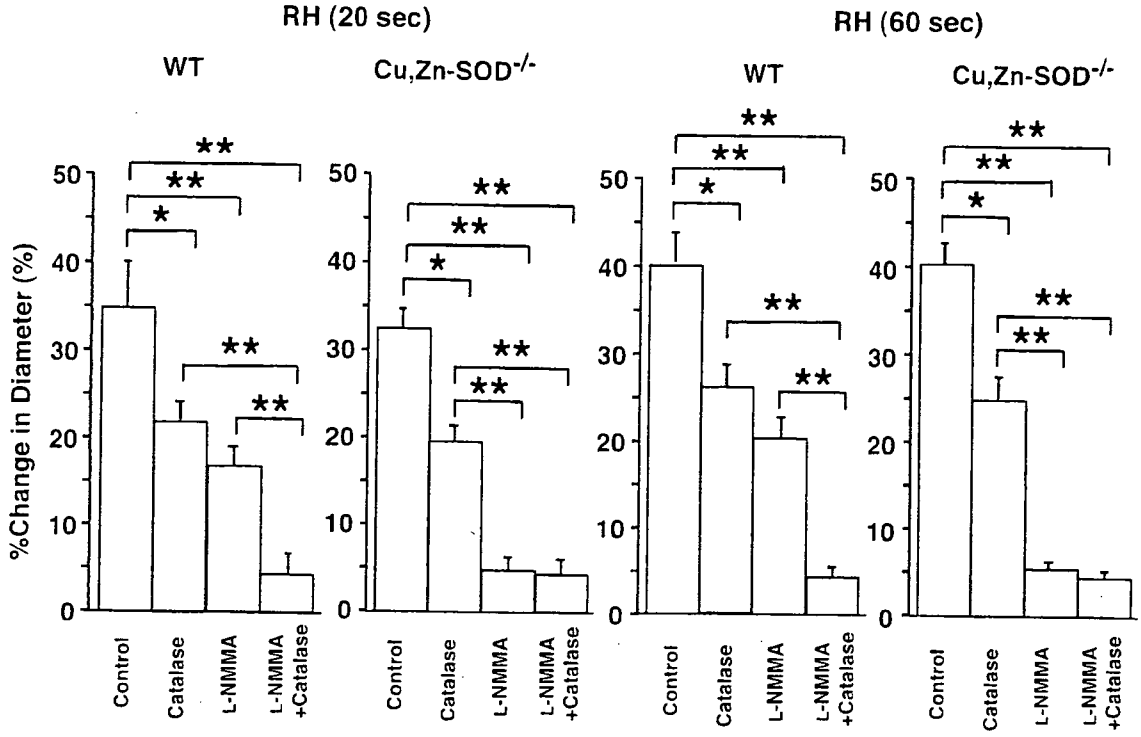


Fig. 1. Mesenteric vasodilatation during reactive hyperemia (RH). In the wild-type (WT) mice, vasodilatation during RH was inhibited by catalase or $N^G$-monomethyl-L-arginine (L-NMMA) and further inhibited by L-NMMA + catalase. In the Cu,Zn-SOD$^{-/-}$ mice (Cu,Zn-SOD$^{-/-}$), vasodilatation during RH was inhibited by catalase and markedly inhibited by L-NMMA, and the remaining response was not inhibited by catalase. The number of arterioles per animals used was 10/5 for each group. *$P < 0.05$; **$P < 0.01$.

*Improvement of ACh-induced vasodilatation by Tempol in Cu,Zn-SOD$^{-/-}$ mice.* It was previously reported that Tempol, a cell membrane-permeable SOD mimetic 4-hydroxy-2,2,6,6-tetramethylpiperidine-*N*-oxyl, decreased oxidative stress in the spontaneously hypertensive rat (31). In the present study, Tempol significantly improved the ACh-induced vasodilatation in Cu,Zn-SOD$^{-/-}$ mice, whereas catalase abolished the beneficial effect of Tempol (Fig. 3), indicating that the effect of Tempol was mediated by endogenous $H_2O_2$ in vivo. In contrast, Tempol had no enhancing effect on the ACh-induced vasodilatation in control mice (Fig. 3), suggesting that a sufficient amount of SOD is present in this strain. In Cu,Zn-SOD$^{-/-}$ mice, L-NMMA did not abolish the ACh-induced vasodilation, and the DCF-DA stain showed remaining fluorescent intensity (Fig. 4). Thus the residual vasodilatation could be caused by the following possible mechanisms. First, NO may also be synthesized in a nonenzymatic manner (27). Nonenzymatic synthesis of NO could occur in the presence of NADPH, glutathione, and L-cysteine, etc., opposing the effects of NOS inhibition (27). Second, the effects of L-NMMA may be limited since it is known that L-NMMA does not abolish NO production (1). $H_2O_2$ produced from vascular smooth muscle cells and other tissues may also contribute to the residual vasodilation (5, 30). Third, the contribution of other proposed

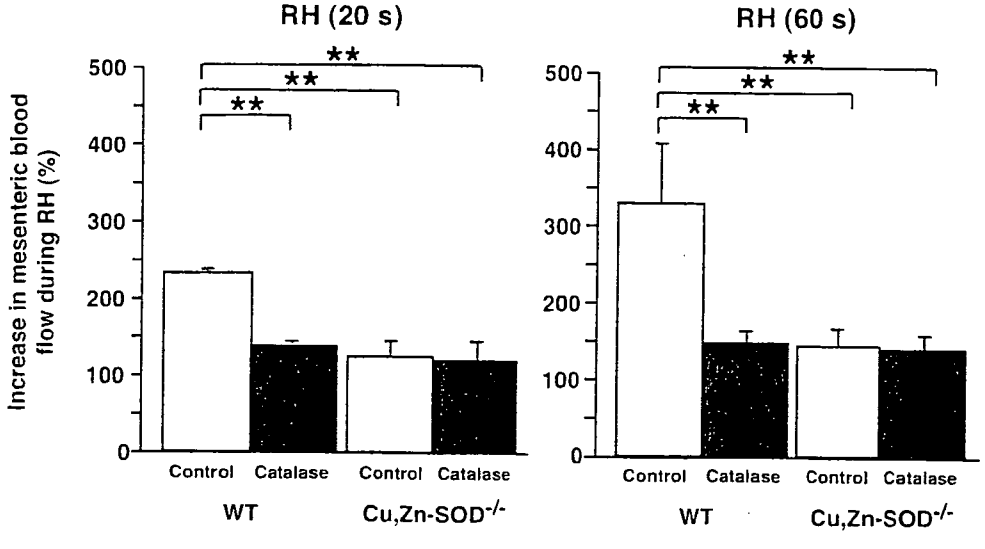


Fig. 2. The increase in mesenteric blood flow during RH. In the presence of indomethacin and L-NMMA, RH-induced increase in blood flow was sensitive to catalase in the WT mice, whereas in the Cu,Zn-SOD$^{-/-}$, the vasodilation was significantly reduced in control and was insensitive to catalase. The number of animals used was 5 for each group. **$P < 0.01$.

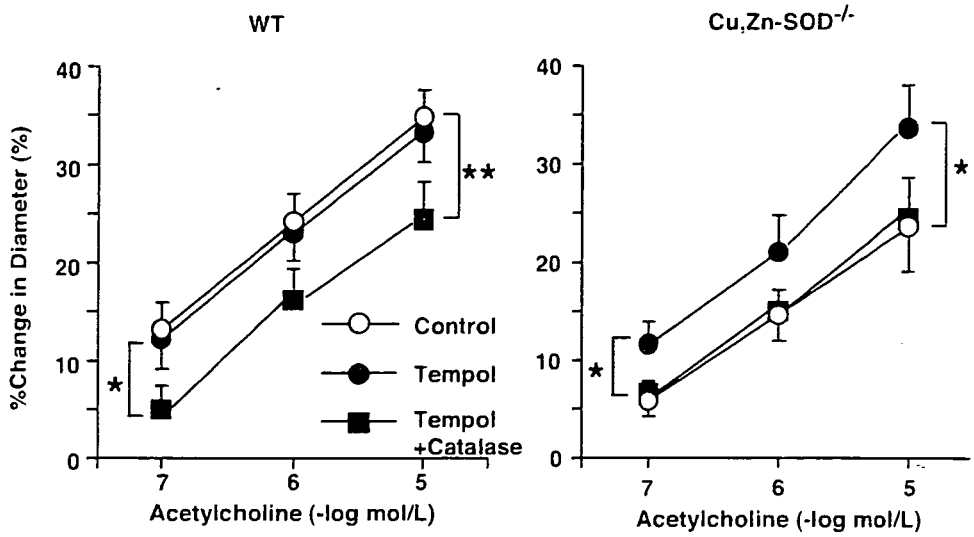


Fig. 3. Endothelium-dependent relaxations to ACh. In the WT mice, endothelium-dependent vasodilatation to ACh (in the presence of indomethacin and L-NMMA) was unchanged with Tempol but significantly inhibited by the addition of catalase. In the Cu,Zn-SOD$^{-/-}$, the vasodilation was significantly enhanced with Tempol, where the response was sensitive to the addition of catalase. The number of arterioles per animals used was 10/5 for each group. *$P$ < 0.05; **$P$ < 0.01.

EDHF candidates, such as $P$-450 metabolites (2, 3) and potassium ion (7), may contribute to the residual vasodilatation. Although RH and ACh have different mechanisms of vasodilator effects, they also share the same flow-induced vasodilator mechanism.

*Endothelium-independent vasodilatation in Cu,Zn-SOD$^{-/-}$ mice.* Microvascular dysfunction in hypercholesterolemic rats was confined to the endothelium because the dilator response to SNP and adenosine was unchanged (37). In the present study, endothelium-independent vasodilatation in response to SNP was comparable between the two genotypes, suggesting that vasodilatation properties of vascular smooth muscle cells were preserved in the Cu,Zn-SOD$^{-/-}$ mice in vivo.

*Detection of vascular $H_2O_2$ and NO production.* Our laboratory (41a) has recently demonstrated that vascular production of $H_2O_2$ and NO after ischemia-reperfusion is enhanced in small coronary arteries and arterioles in vivo, respectively. It was previously shown that a ACh-induced increase in fluorescence intensity in endothelial cells of the mesenteric artery is significantly reduced in Cu,Zn-SOD$^{-/-}$ mice (25). In the present study, vascular $H_2O_2$ production, as assessed by DCF-DA fluorescent intensity in mesenteric arterioles, was markedly impaired

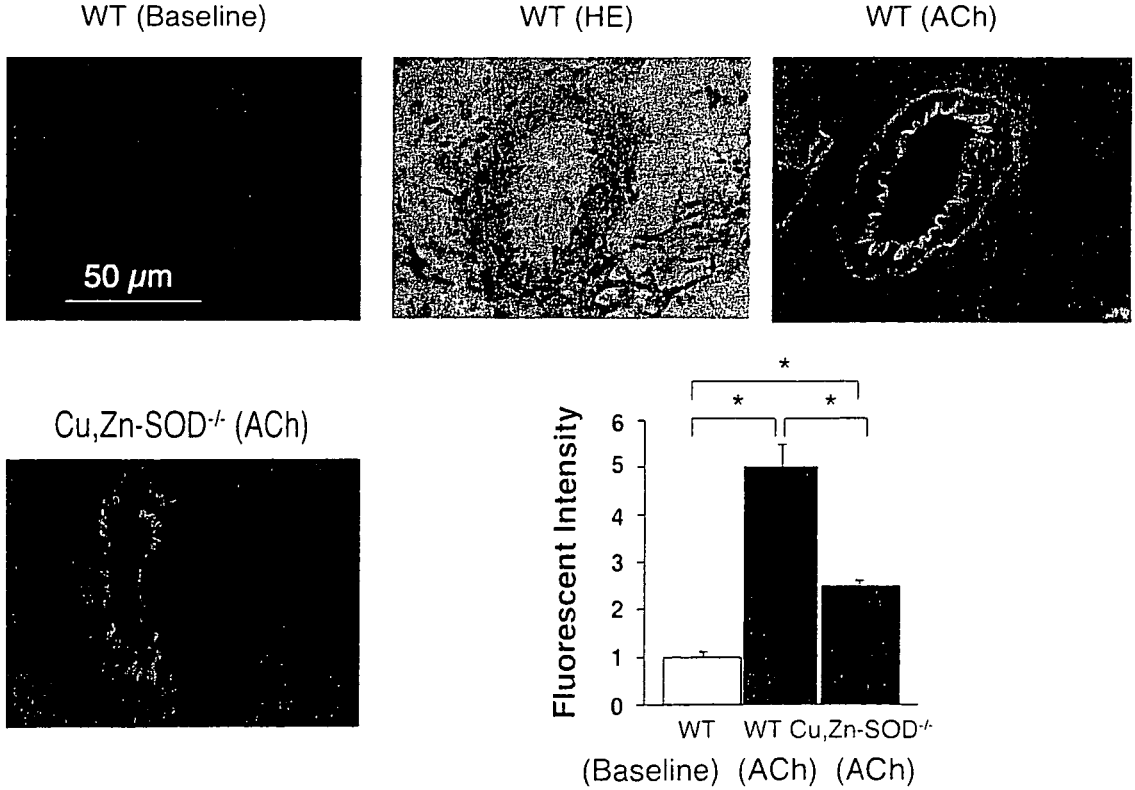


Fig. 4. Detection of vascular $H_2O_2$ production. Vascular $H_2O_2$ production in mesenteric arterioles was significantly increased in response to ACh in WT mice but markedly impaired in Cu,Zn-SOD$^{-/-}$. The number of arterioles per animals used was 10/5 for each group. *$P$ < 0.05. HE, Hematoxylin eosin.

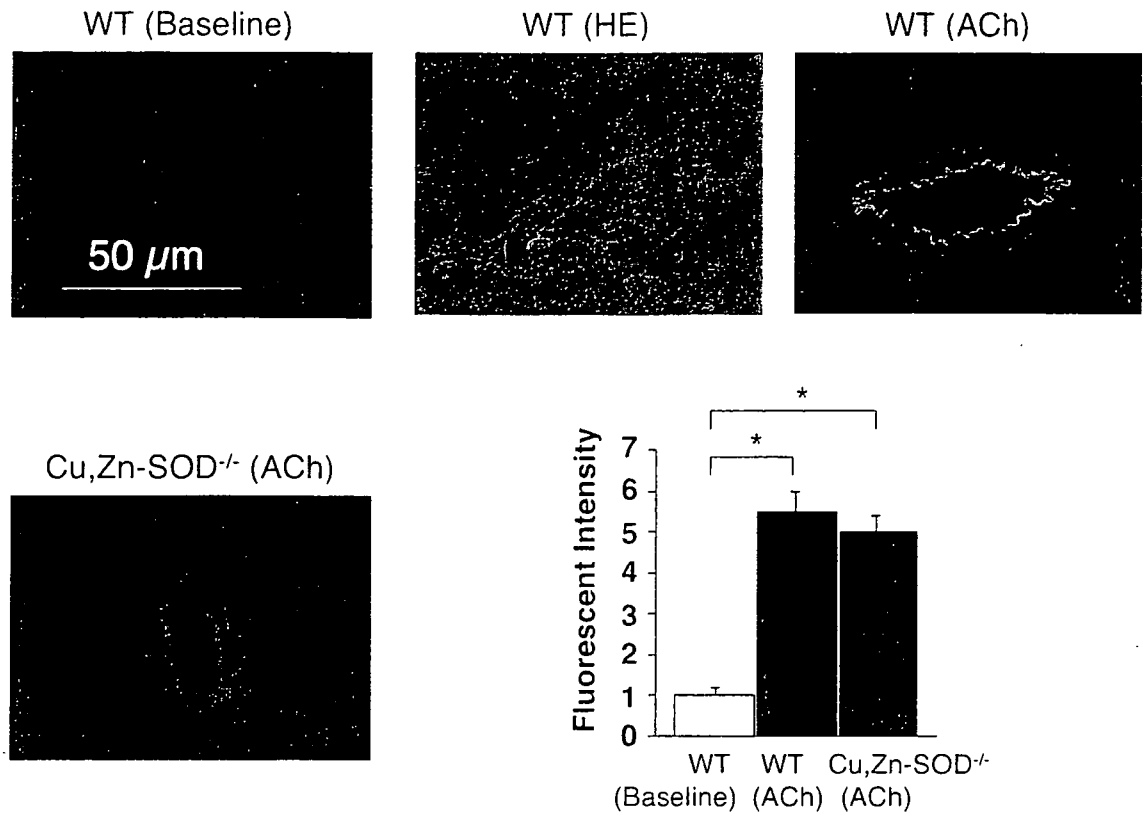


Fig. 5. Detection of vascular nitric oxide (NO) production. Vascular NO production in mesenteric arterioles was significantly increased in response to ACh in WT mice and unaltered in Cu,Zn-SOD$^{-/-}$. The number of arterioles per animals used was 10/5 for each group. *$P < 0.05$.

in Cu,Zn-SOD$^{-/-}$ mice (Fig. 4). These findings indicate that endothelial production of $H_2O_2$ is significantly impaired in Cu,Zn-SOD$^{-/-}$ mice, confirming the importance of the enzyme in endothelial synthesis of $H_2O_2$.

In the previous study by Morikawa et al. (25), eNOS protein expression was comparable between Cu,Zn-SOD$^{-/-}$ and wild-type mice. In the present study, vascular NO production in small mesenteric artery was unaltered in Cu,Zn-SOD$^{-/-}$ mice compared with wild-type mice (Fig. 5). NO could compensate for the loss of action of $H_2O_2$, although there are still many uncertainties about the local cellular dynamics of superoxide anions and NO.

*Study limitations.* Several limitations should be mentioned for the present study. First, we estimated blood flow in the mesenteric circulation using microspheres. We were unable to calculate the absolute values of local blood flow or shear stress because of the methodological limitations. However, since the flow measurement with microspheres was performed at the end of the experiments, it should not have influenced other results. Second, we used Cu,Zn-SOD$^{-/-}$ mice in the present study, where unknown compensatory mechanisms may be operative, and we were unable to elucidate the mechanism(s) for the remaining EDHF-mediated responses in those mice.

*Clinical implications.* RH is an important regulatory mechanism of the cardiovascular system, reflecting the flow reserve in response to a brief period of cessation of flow. An impaired flow reserve in resistance vessels is a hallmark of microvascular dysfunction with coronary risk factors. Hypertension is associated with structural alterations in the microcirculation and a reduced endothelium-dependent dilation in conduit arteries (19). It is well known that abnormality in Cu,Zn-SOD is noted in several diseases, including hypertension and diabetes mellitus (36, 39).

In conclusion, endogenous $H_2O_2$ exerts important vasodilator effects of mesenteric smaller arterioles during RH, especially at the low level of NO, and that Cu,Zn-SOD plays an important role in the synthesis of endogenous $H_2O_2$ during RH in vivo.

## GRANTS

This work was supported in part by the Japanese Ministry of Education, Science, Sports, Culture, and Technology (Tokyo, Japan) Grants 16209027 (to H. Shimokawa), 16300164, and 19300167 (to T. Yada), the Program for Promotion of Fundamental Studies in Health Sciences of the Organization for Pharmaceutical Safety and Research of Japan (to H. Shimokawa), and Takeda Science Foundation 2002 (to T. Yada).

## REFERENCES

1. **Amezcua JL, Palmer RM, de Souza BM, Moncada S.** Nitric oxide synthesized from L-arginine regulates vascular tone in the coronary circulation of the rabbit. *Br J Pharmacol* 97: 1119–1124, 1989.
2. **Bauersachs J, Hecker M, Busse R.** Display of the characteristics of endothelium-derived hyperpolarizing factor by a cytochrome P450-derived arachidonic acid metabolite in the coronary microcirculation. *Br J Pharmacol* 113: 1548–1553, 1994.
3. **Campbell WB, Gebremedhin D, Pratt PF, Harder DR.** Identification of epoxyeicosatrienoic acids as an endothelium-derived hyperpolarizing factor. *Circ Res* 78: 415–423, 1996.
4. **Chen G, Suzuki H, Weston AH.** Acetylcholine releases endothelium-derived hyperpolarizing factor and EDRF from blood vessels. *Br J Pharmacol* 95: 1165–1174, 1988.
5. **Chen Y, Pearlman A, Luo Z, Wilcox CS.** Hydrogen peroxide mediates a transient vasorelaxation with Tempol during oxidative stress. *Am J Physiol Heart Circ Physiol* 293: H2085–H2092, 2007.

6. **Coffman JD, Gregg DE.** Reactive hyperemia characteristics of the myocardium. *Am J Physiol* 199: 1143–1149, 1960.
7. **Edwards G, Dora KA, Gardener MJ, Garland CJ, Weston AH.** $K^+$ is an endothelium-derived hyperpolarizing factor in rat arteries. *Nature* 396: 269–272, 1998.
8. **Feletou M, Vanhoutte PM.** Endothelium-dependent hyperpolarization of canine smooth muscle. *Br J Pharmacol* 93: 515–524, 1988.
9. **Feletou M, Vanhoutte PM.** Endothelium-derived hyperpolarizing factor: where are we now? *Arterioscler Thromb Vasc Biol* 26: 1215–1225, 2006.
10. **Gupte SA, Rupawalla T, Mohazzab-H KM, Wolin MS.** Regulation of NO-elicited pulmonary artery relaxation and guanylate cyclase activation by NADH oxidase and SOD. *Am J Physiol Heart Circ Physiol* 276: H1535–H1542, 1999.
11. **Kanatsuka H, Sekiguchi N, Sato K, Akai K, Wang Y, Komaru T, Ashikawa K, Takishima T.** Microvascular sites and mechanisms responsible for reactive hyperemia in the coronary circulation of the beating canine heart. *Circ Res* 71: 912–922, 1992.
12. **Kitakaze M, Hori M, Takashima S, Iwai K, Sato H, Inoue M, Kitabatake A, Kamada T.** Superoxide dismutase enhances ischemia-induced reactive hyperemic flow and adenosine release in dogs. A role of 5′-nucleotidase activity. *Circ Res* 71: 558–566, 1992.
13. **Kiyooka T, Hiramatsu O, Shigeto F, Nakamoto H, Tachibana H, Yada T, Ogasawara Y, Kajiya M, Morimoto T, Morizane Y, Mohri S, Shimizu J, Ohe T, Kajiya F.** Direct observation of epicardial coronary capillary hemodynamics during reactive hyperemia and during adenosine administration by intravital video microscopy. *Am J Physiol Heart Circ Physiol* 288: H1437–H1443, 2005.
14. **Kobayashi N, Kobayashi K, Kouno K, Horinaka S, Yagi S.** Effects of intra-atrial injection of colored microspheres on systemic hemodynamics and regional blood flow in rats. *Am J Physiol Heart Circ Physiol* 266: H1910–H1917, 1994.

14a. **Koller A, Bagi Z.** Nitric oxide and $H_2O_2$ contribute to reactive dilation of isolated coronary arterioles. *Am J Physiol Heart Circ Physiol* 287: H2461–H2467, 2004.

15. **Koller A, Sun D, Kaley G.** Role of shear stress and endothelial prostaglandins in flow- and viscosity-induced dilation of arterioles in vitro. *Circ Res* 72: 1276–1284, 1993.
17. **Kopkan L, Castillo A, Navar LG, Majid DS.** Enhanced superoxide generation modulates renal function in ANG II-induced hypertensive rats. *Am J Physiol Renal Physiol* 290: F80–F86, 2006.
18. **Kuo L, Davis MJ, Chilian WM.** Endothelium-dependent, flow-induced dilation of isolated coronary arterioles. *Am J Physiol Heart Circ Physiol* 259: H1063–H1070, 1990.
19. **Lauer T, Heiss C, Preik M, Balzer J, Hafner D, Strauer BE, Kelm M.** Reduction of peripheral flow reserve impairs endothelial function in conduit arteries of patients with essential hypertension. *J Hypertens* 23: 563–569, 2005.

19a. **Matoba T, Shimokawa H, Kubota H, Morikawa K, Fujiki T, Kunihiro I, Mukai Y, Hirakawa Y, Takeshita A.** Hydrogen peroxide is an endothelium-derived hyperpolarizing factor in human mesenteric arteries. *Biochem Biophys Res Commun* 290: 909–913, 2002.

19b. **Matoba T, Shimokawa H, Morikawa K, Kubota H, Kunihiro I, Urakami-Harasawa L, Mukai Y, Hirakawa Y, Akaike T, Takeshita A.** Electron spin resonance detection of hydrogen peroxide as an endothelium-derived hyperpolarizing factor in porcine coronary microvessels. *Arterioscler Thromb Vasc Biol* 23: 1224–1230, 2003.

20. **Matoba T, Shimokawa H, Nakashima M, Hirakawa Y, Mukai Y, Hirano K, Kanaide H, Takeshita A.** Hydrogen peroxide is an endothelium-derived hyperpolarizing factor in mice. *J Clin Invest* 106: 1521–1530, 2000.
23. **Miura H, Bosnjak JJ, Ning G, Saito T, Miura M, Gutterman DD.** Role for hydrogen peroxide in flow-induced dilation of human coronary arterioles. *Circ Res* 92: e31–e40, 2003.
24. **Mori H, Haruyama S, Shinozaki Y, Okino H, Iida A, Takanashi R, Sakuma I, Husseini WK, Payne BD, Hoffman JI.** New nonradioactive microspheres and more sensitive X-ray fluorescence to measure regional blood flow. *Am J Physiol Heart Circ Physiol* 263: H1946–H1957, 1992.

24a. **Morikawa K, Fujiki T, Matoba T, Kubota H, Hatanaka M, Takahashi S, Shimokawa H.** Important role of superoxide dismutase in EDHF-mediated responses of human mesenteric arteries. *J Cardiovasc Pharmacol* 44: 552–556, 2004.

25. **Morikawa K, Shimokawa H, Matoba T, Kubota H, Akaike T, Talukder MA, Hatanaka M, Fujiki T, Maeda H, Takahashi S, Takeshita A.** Pivotal role of Cu,Zn-superoxide dismutase in endothelium-dependent hyperpolarization. *J Clin Invest* 112: 1871–1879, 2003.
27. **Moroz LL, Norby SW, Cruz L, Sweedler JV, Gillette R, Clarkson RB.** Non-enzymatic production of nitric oxide (NO) from NO synthase inhibitors. *Biochem Biophys Res Commun* 253: 571–576, 1998.
28. **Olsson RA.** Myocardial reactive hyperemia. *Circ Res* 37: 263–270, 1975.
29. **Pawlik WW, Obuchowicz R, Pawlik MW, Sendur R, Biernat J, Brzozowski T, Konturek SJ.** Histamine $H_3$ receptors modulate reactive hyperemia in rat gut. *J Physiol Pharmacol* 55: 651–661, 2004.
30. **Saitoh S, Zhang C, Tune JD, Potter B, Kiyooka T, Rogers PA, Knudson JD, Dick GM, Swafford A, Chilian WM.** Hydrogen peroxide: a feed-forward dilator that couples myocardial metabolism to coronary blood flow. *Arterioscler Thromb Vasc Biol* 26: 2614–2621, 2006.
31. **Schnackenberg CG, Wilcox CS.** Two-week administration of Tempol attenuates both hypertension and renal excretion of 8-Iso prostaglandin $F_{2alpha}$. *Hypertension* 33: 424–428, 1999.
32. **Shimokawa H.** Primary endothelial dysfunction: atherosclerosis. *J Mol Cell Cardiol* 31: 23–37, 1999.
33. **Takamura Y, Shimokawa H, Zhao H, Igarashi H, Egashira K, Takeshita A.** Important role of endothelium-derived hyperpolarizing factor in shear stress-induced endothelium-dependent relaxations in the rat mesenteric artery. *J Cardiovasc Pharmacol* 34: 381–387, 1999.
34. **Taylor HJ, Chaytor AT, Evance WH, Griffith TM.** Inhibition of the gap junctional component of endothelium-dependent relaxations in rabbit iliac artery by 18-alpha glycyrrhetinic acid. *Br J Pharmacol* 125: 1–3, 1998.
35. **Tsunoda R, Okumura K, Ishizaka H, Matsunaga T, Tabuchi T, Tayama S, Yasue H.** Enhancement of myocardial reactive hyperemia with manganese-superoxide dismutase: role of endothelium-derived nitric oxide. *Cardiovasc Res* 31: 537–545, 1996.
36. **Uchimura K, Nagasaka A, Hayashi R, Makino M, Nagata M, Kakizawa H, Kobayashi T, Fujiwara K, Kato T, Iwase K, Shinohara R, Kato K, Itoh M.** Changes in superoxide dismutase activities and concentrations and myeloperoxidase activities in leukocytes from patients with diabetes mellitus. *J Diabetes Complications* 13: 264–270, 1999.
37. **VanTeeffelen JW, Constantinescu AA, Vink H, Spaan JA.** Hypercholesterolemia impairs reactive hyperemic vasodilation of 2A but not 3A arterioles in mouse cremaster muscle. *Am J Physiol Heart Circ Physiol* 289: H447–H454, 2005.
38. **Wolin MS, Rodenburg JM, Messina EJ, Kaley G.** Similarities in the pharmacological modulation of reactive hyperemia and vasodilation to hydrogen peroxide in rat skeletal muscle arterioles: effects of probes for endothelium-derived mediators. *J Pharmacol Exp Ther* 253: 508–512, 1990.
39. **Wu R, Millette E, Wu L, de Champlain J.** Enhanced superoxide anion formation in vascular tissues from spontaneously hypertensive and desoxycorticosterone acetate-salt hypertensive rats. *J Hypertens* 19: 741–748, 2001.
40. **Yada T, Hiramatsu O, Kimura A, Goto M, Ogasawara Y, Tsujioka K, Yamamori S, Ohno K, Hosaka H, Kajiya F.** In vivo observation of subendocardial microvessels of the beating porcine heart using a needle-probe videomicroscope with a CCD camera. *Circ Res* 72: 939–946, 1993.
41. **Yada T, Hiramatsu O, Kimura A, Tachibana H, Chiba Y, Lu S, Goto M, Ogasawara Y, Tsujioka K, Kajiya F.** Direct in vivo observation of subendocardial arteriolar response during reactive hyperemia. *Circ Res* 77: 622–631, 1995.

41a. **Yada T, Shimokawa H, Hiramatsu O, Haruna Y, Morita Y, Kashihara N, Shinozaki Y, Mori H, Goto M, Ogasawara Y, Kajiya F.** Cardioprotective role of endogenous hydrogen peroxide during ischemia-reperfusion injury in canine coronary microcirculation in vivo. *Am J Physiol Heart Circ Physiol* 291: H1138–H1146, 2006.

42. **Yada T, Shimokawa H, Hiramatsu O, Kajita T, Shigeto F, Goto M, Ogasawara Y, Kajiya F.** Hydrogen peroxide, an endogenous endothelium-derived hyperpolarizing factor, plays an important role in coronary autoregulation in vivo. *Circulation* 107: 1040–1045, 2003.
44. **Yada T, Shimokawa H, Hiramatsu O, Shinozaki Y, Mori H, Goto M, Ogasawara Y, Kajiya F.** Important role of endogenous hydrogen peroxide in pacing-induced metabolic coronary vasodilatation in dogs in vivo. *J Am Coll Cardiol* 50: 1272–1278, 2007.
45. **Zhang DX, Gutterman DD.** Mitochondrial reactive oxygen species-mediated signaling in endothelial cells. *Am J Physiol Heart Circ Physiol* 292: H2023–H2031, 2007.

BRAIN RESEARCH 1158 (2007) 116-122

available at www.sciencedirect.com

ScienceDirect

www.elsevier.com/locate/brainres

BRAIN RESEARCH

Research Report

# Simultaneous observation of superficial cortical and intracerebral microvessels in vivo during reperfusion after transient forebrain ischemia in rats using synchrotron radiation

*Masanori Morita*, Motohisa Ohkawa, Shuhei Miyazaki, Tsuyoshi Ishimaru, Keiji Umetani[1], Koichiro Suzuki*

*Department of Acute Medicine, Kawasaki Medical School, 577 Matsushima, Kurashiki, Okayama 701-0192, Japan*

ARTICLE INFO

*Article history:*
Accepted 21 April 2007
Available online 4 May 2007

*Keywords:*
Synchrotron radiation
Transient ischemia
Reperfusion
Pial arteriole
Striate artery

ABSTRACT

Using a newly developed angiography system that combines monochromatic synchrotron radiation (MSR) as an X-ray source with a high-definition camera or video system, we observed superficial cortical and intracerebral microvessels simultaneously in vivo during reperfusion after transient forebrain ischemia. Transient brain ischemia was induced by 10-min four-vessel occlusion in rats under general anesthesia. Angiographic images were then sequentially obtained at 3 frames/s. The detector features a 7-μm equivalent pixel size projected onto the input area and a 7 mm×7 mm input field. Changes in the cerebral microvessels were observed before and 1, 5, 10, 15, 20 and 30 min after transient cerebral ischemia using the MSR angiography system. The calibers of the internal carotid artery (ICA), middle cerebral artery (MCA), and striate artery (SA) significantly increased 1 min after reperfusion, while the pial arteriole (PA) caliber significantly decreased (76% of base line). The MCA, PA and SA were significantly dilated 5 and 10 min after reperfusion. Although the caliber of the ICA significantly decreased after 30 min reperfusion compared with the basal value, the calibers of the other three vessels remained larger than the basal values throughout the experiment. Early venous filling was observed at 5 and 10 min after reperfusion. The MSR angiography system is useful for investigating morphological changes in both cortical and central branches of cerebral vessels in rats during reperfusion after cerebral ischemia.



## 1. Introduction

A rapid postischemic increase in cerebral blood flow relative to control values, i.e., hyperperfusion, has long been documented in animal stroke models, and hyperperfusion is the hallmark of efficient reopening of occluded arteries with subsequent reperfusion of the tissue (Marchal et al., 1999). Recognition of the actual behaviors of cerebral vessels during ischemia and reperfusion is the first step to understanding the pathophysiologic events of the brain suffering from ischemic injury (Ginsberg et al., 1997). Various methods have been used to achieve morphological observation of the cerebral vessels

* *Corresponding author.* Fax: +81 86 464 1044.
E-mail address: nubo@fj8.so-net.ne.jp (M. Morita).
[1] Research and Utilization Division, Japan Synchrotron Radiation Research Institute, SPring-8, Mikazuki, Sayo, Hyogo, Japan.

0006-8993/$ – see front matter © 2007 Elsevier B.V. All rights reserved.
doi:10.1016/j.brainres.2007.04.060

Table 1

| | Before ischemia | During ischemia | After ischemia | | | | | |
|---|---|---|---|---|---|---|---|---|
| | | | 1 min | 5 min | 10 min | 15 min | 20 min | 30 min |
| MABP (mmHg) | 102±11 | 37±20 | 99±11 | 109±12 | 108±14 | 107±12 | 107±11 | 104±12 |

Data are means±SD. MABP: mean arterial blood pressure.

during ischemia and reperfusion, with each having its merits and demerits. In animal models, pial microvessels are accessible by direct visualization using a cranial window technique equipped with confocal laser microscopy/fluorescence video imaging, but only to a depth of 250 μm from the cortical surface (Villringer et al., 1989). However, deeper microvascular beds such as those of the striate artery, which are not accessible with the cranial window technique, can be assessed using tracer perfusion techniques and reconstruction by computer-assisted static image analysis for study (del Zoppo et al., 1991). However, passage of all currently used tracers through the blood–brain barrier is limited, and as a consequence a nonlinear relationship between tracer uptake and true cerebral blood flow is observed. Accordingly, for study of ischemic injuries these techniques for direct visualization of microvascular beds in the brain allow only restricted observations of real-time events on the cortical surface and the basilar artery.

A new angiography system, consisting of monochromatic synchrotron radiation (MSR) as an X-ray source and a high-definition camera with a video system as a detector, has been developed in Hyogo, Japan (Umetani et al., 2002). This angiography system uses nearly parallel X-rays. Consequently, it can visualize microvessels with a caliber of 20–30 μm (Kidoguchi et al., 2006; Tokiya et al., 2004). Conventional X-ray imaging with an X-ray tube can depict only vessels with a caliber larger than 200 μm. This new system, therefore, offers higher resolution. In this study, we attempted in vivo simultaneous observation of pial arterioles and striate arteries in rats during reperfusion after transient forebrain ischemia using this MSR angiography system.

## 2. Results

### 2.1. *Physiological variables*

Six rats attained forebrain ischemia, but two did not. The mean arterial blood pressure (ABP) significantly increased by 135±18% during ischemia and then returned to its basal level immediately after reperfusion. There was no significant change in mean ABP while microangiography was performed (Table 1). The arterial blood gas levels were not significantly different 15 min before ischemia and 30 min after reperfusion (Table 2).

Table 2

| | Before ischemia | After ischemia |
|---|---|---|
| pH | 7.405±0.02 | 7.397±0.03 |
| $PaO_2$, mmHg | 89±4 | 87±4 |
| $PaCO_2$, mmHg | 38.1±2.7 | 39.1±3.4 |
| Na, mmol/l | 140±2 | 139±2 |
| K, mmol/l | 4.0±0.3 | 4.2±0.4 |
| Hematocrit, % | 46.2±1.5 | 43.2±1.9 |

Data are means±SD. $PaO_2$: arterial oxygen partial pressure; $PaCO_2$: arterial carbon dioxide partial pressure; Na: sodium concentration in serum; K: potassium concentration in serum.

### 2.2. *Basal conditions*

The diagram in Fig. 1 demonstrates the stereotactic co-ordinates of the image field of view in the rat brain. The MSR angiography system could detect a tungsten wire 100 μm in diameter and provided good visibility of the ICA, MCA, PA and SA under basal conditions (Fig. 2A). Each image in Figs. 2A–D depicts a temporal subtraction result for flat-field correction; the image taken before injection was subtracted from raw images taken after injection to eliminate the superimposed background structure. This system could also detect microvessels with a caliber of 20–30 μm. The mean ICA caliber was 401±44 μm, the mean MCA caliber was 179±21 μm, the mean PA caliber was 64±14 μm and the mean SA caliber was 53±18 μm.

### 2.3. *Reperfusion*

The ICA caliber significantly increased at 1 min after reperfusion, as shown in Fig. 2B, and those of the MCA and SA significantly increased at 1, 5 and 10 min after

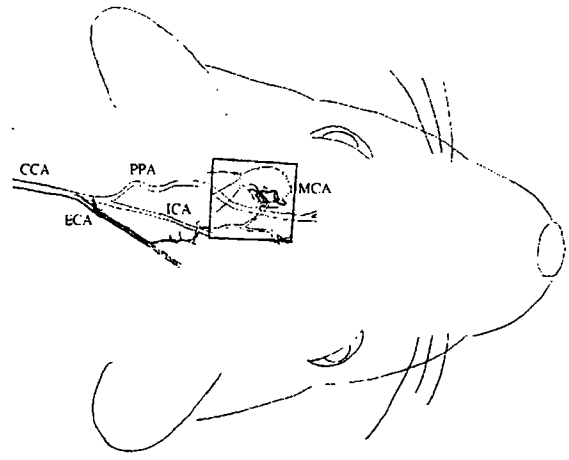


**Fig. 1 – Diagram showing stereotactic co-ordinates of the image field of view in the rat brain. The quadrangular area of 7 mm×7 mm in the diagram is the area included in the photograph. CCA, common carotid artery; ECA, external carotid artery; PPA, pterygopalatine artery; ICA, internal carotid artery; MCA, middle cerebral artery.**

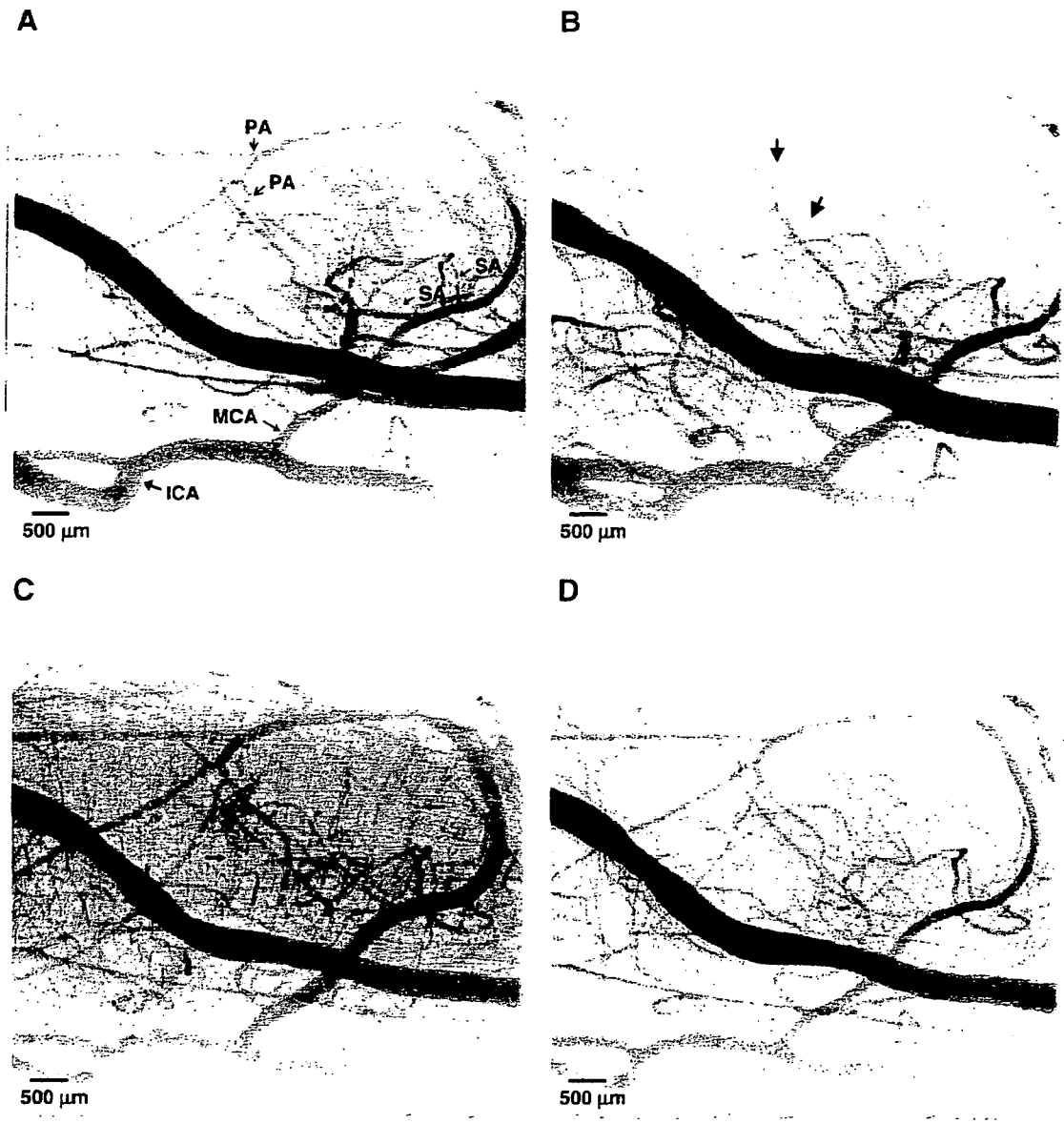


**Fig. 2 – (A) Digitally subtracted images of monochromatic synchrotron radiation microangiography of normal rat cerebral arteries. ICA: internal carotid artery; MCA: middle cerebral artery; PA: pial arteriole; and SA: striate artery. (B) Images obtained at 1 min after reperfusion. Pial arterioles were significantly constricted (arrows). In contrast, ICA, MCA and striate arteries were significantly dilated at 1 min after reperfusion. (C) Images obtained at 10 min after reperfusion. Pial arterioles, MCA and striate arteries remained dilated. Early venous filling was observed (arrows). (D) Images obtained at 30 min after reperfusion. The ICA caliber was significantly decreased, but the other three vessels had returned to basal values.**

reperfusion, as shown in Figs. 2B and C. The extent of vasodilatation immediately after reperfusion (at 1 min) was 130% for the ICA, 160% for the MCA and 140% for the SA ($p<0.005$). In contrast, at 1 min after reperfusion ($p<0.00001$), the PA caliber statistically significantly decreased by 24%, and thereafter statistically significantly increased at 5 and 10 min after reperfusion, as shown in Figs. 2B and C. The calibers of these vessels tended to return to base line values at 15 min after reperfusion, as shown in Figs. 3, 4 and 5. Although the ICA caliber at 30-min reperfusion had significantly decreased as compared with the basal value, as shown in Fig. 6, the other three vessel calibers were above their basal values throughout the experiment. As shown in Fig. 2C, early venous filling was observed at 5 and 10 min after reperfusion.

## 3. Discussion

We successfully observed in vivo morphological changes in both cortical and central branches of cerebral vessels in rats during reperfusion after cerebral ischemia using the MSR